ELSEVIER

Chemical Geology 240 (2007) 129–150

CHEMICAL GEOLOGY
INCLUDING
ISOTOPE GEOSCIENCE

www.elsevier.com/locate/chemgeo

Olivine-hosted melt inclusions and melting processes beneath the FAMOUS zone (Mid-Atlantic Ridge)

Muriel Laubier [a,*], Pierre Schiano [a], Régis Doucelance [a], Luisa Ottolini [b], Didier Laporte [a]

[a] *Laboratoire Magmas et Volcans, CNRS-UMR6524, IRD-M163, 5 rue Kessler, 63038 Clermont-Ferrand, France*
[b] *Istituto di Geoscienze e Georisorse (IGG), Sede di Pavia-CNR, via Ferrata 1, 27100 Pavia, Italy*

Received 24 July 2006; received in revised form 10 January 2007; accepted 3 February 2007

Editor: S.L. Goldstein

Abstract

Major- and trace-element abundances have been obtained for olivine-hosted melt inclusions from a picritic basalt (ARP73–10–03) dredged in the FAMOUS locality along the Northern Mid-Atlantic Ridge. Isolated in homogeneous, highly primitive olivine phenocrysts ($Fo_{87.2–91.3}$), melt inclusions provide important information about the processes of melt generation beneath mid-ocean ridges. They contain near-primary magmas that display a large range of major- and trace-element compositions and form a primitive continuation of the FAMOUS whole rock suites. Both slightly depleted and enriched melt inclusions can be distinguished on the basis of their trace-element compositions, with $(La/Sm)_N$ ratios ranging from 0.58 to 1.52.

Melt inclusions display chemical trends on both major- and trace-element variation diagrams, indicating that they constitute a suite of genetically-related, highly primitive magmas. The evolution of the melt inclusions is inconsistent with a model of mantle-melt chemical exchange during reactive transport, suggesting that the trapped melts are able to preserve pristine information about the melting process and/or source composition. Comparison of these trends with predicted curves for models of peridotite melting indicates that compositional variations are best reproduced by polybaric partial melting of a relatively homogeneous mantle source and subsequent mixing in various proportions of the melt batches produced at different degrees of melting and/or in different parts of the melting system. These observations require that transport of melts from the melting region to the site of olivine crystallization occurs without significant chemical exchange with the surrounding mantle.

Keywords: Melt inclusions; Olivine; Mid-ocean ridge basalts; Mantle melting

1. Introduction

Melt generation at mid-ocean ridges involves polybaric melting of an adiabatically upwelling mantle and is thought to begin in the garnet peridotite field (e.g., Salters and Hart, 1989). After correction for low-pressure fractionation, major-element systematics of MORB (mid-ocean ridge basalts) have been explained in terms of variation of the potential mantle temperature which controls the initial pressure of melting of a compositionally uniform source (Klein and Langmuir, 1987; McKenzie and Bickle, 1988; Langmuir et al., 1992; Plank and Langmuir, 1992). Alternative models have attributed the

* Corresponding author. Postdoctoral Fellow Harvard University, Department of Earth and Planetary Sciences, 20 Oxford Street Cambridge, MA 02138. Tel.: +1 617 496 6924; fax: +1 617 496 6958.
E-mail address: laubier@eps.harvard.edu (M. Laubier).

0009-2541/$ - see front matter © 2007 Elsevier B.V. All rights reserved.
doi:10.1016/j.chemgeo.2007.02.002

variability in the major-element compositions of MORB to variations in the final pressure of melting controlled by cooling at the surface, and to heterogeneous source compositions, with only modest potential temperature variations (Niu and Batiza, 1991, 1993; Shen and Forsyth, 1995; Presnall et al., 2002). On the other hand, models for MORB generation based on trace elements and isotopic systematics have emphasized the role of a heterogeneous upper mantle in controlling the chemical variations. This heterogeneity may include regional chemical and isotopic gradients along mid-ocean ridges, reflecting the influence of nearby plumes (Schilling, 1973), as well as ubiquitous minor isotopic variations in the mantle related to the presence of stretched strips of subducted oceanic crust through a 'marble-cake' structure (Allègre and Turcotte, 1986).

Compositions of MORB samples thus record the chemical fingerprint of several factors, such as variation in the source composition, in the degree of partial melting, potential temperature heterogeneity, melt extraction, migration towards the surface, and low-pressure differentiation. Investigation of the effects of melting and source variation on the small-scale chemical variation in MORB therefore requires only the most primitive samples, or those which have been corrected for low-pressure fractionation. Characterizing instantaneous melts preserved as glass inclusions in minerals offers a powerful perspective on this problem, as inclusions in early-formed crystals may sample a range of primitive liquids that did not suffer homogenization or fractionation, for instance, in shallow magma chambers. They can therefore be used to assess variations in the mantle source composition and various aspects of MORB generation, such as the degree of melting, the style of melt transport and the effects of re-equilibration and mixing of melt batches (see Sobolev, 1996; Schiano, 2003 and references therein).

In the present study, we report major- and trace-element compositions of a series of near-primary magmas of MORB preserved as inclusions in high-Mg olivines from a picritic basalt from the FAMOUS zone, Northern Mid-Atlantic Ridge. The data will be shown to provide important information on the nature of melting processes beneath the ridge. In particular, they demonstrate that primitive melt inclusions from a single sample can preserve a large compositional range that can be modeled by isentropic continuous melting of a homogeneous mantle source.

2. Sample description

Primitive olivine-hosted melt inclusions from a MORB (ARP73–10–03) dredged at the FAMOUS zone (Northern Mid-Atlantic Ridge, 36°8372′N, 33°2482′W) were analyzed. Compositional characteristics of whole rocks from the FAMOUS area suggest a large range of parental magmas (Langmuir et al., 1977; White and Bryan, 1977; Bryan, 1979; Le Roex et al., 1981; Frey et al., 1993) as a result of dynamic melting (Langmuir et al., 1977) and low-pressure crystallization (Bender et al., 1978; Frey et al., 1993). This area is part of a geochemical anomaly along the Mid-Atlantic Ridge (31–41°N) associated with the Azores hotspot (Dosso et al., 1999). In addition, small-scale heterogeneity of the upper mantle beneath the FAMOUS zone has been identified from Pb and Os isotopic compositions of whole rocks and sulfide globules (Dupré et al., 1981; Roy-Barman et al., 1998).

The ARP73–10–03 sample is a picrite containing more than 20% olivine phenocrysts (1–5 mm; $Fo_{87.2–91.3}$), rare clinopyroxene (~1 mm) and plagioclase xenocrysts with typical rounded shapes, abundant spinel as inclusions in olivines or as discrete crystals in the groundmass (Kamenetsky, 1996) and a hyalocrystalline groundmass composed mainly of glass, plagioclase ($An_{75–80}$) and olivine microlites (~Fo_{86}). The picritic composition of the host rock (MgO=24 wt.%) is not representative of a pristine magma and essentially reflects mechanical accumulation of olivine (Le Roex et al., 1981), a hypothesis further supported by Os isotope compositions of the constituent phases of the sample (Gannoun et al., 2004).

Primary glass inclusions, randomly dispersed in olivine phenocrysts, are sub-spherical (10–300 μm in diameter) and generally have negative crystal shapes with planar facets and rounded edges (Fig. 1). The absence of minute daughter minerals in the inclusions and the rareness of thermal shrinkage bubbles give evidence for fast cooling by quenching of the host crystals. Primary glass inclusions have also been found within Cr-spinels in the ARP73–10–03 MORB (Kamenetsky, 1996).

3. Analytical techniques

3.1. Electron microprobe analysis

Major-element compositions of melt inclusions and host olivines were measured with a CAMECA SX 100 microprobe at the Laboratoire Magmas et Volcans. The following routine was used for glass (peak counting times are given for each element): an accelerating voltage of 15 kV, a sample current of 8 nA for Na (20 s), Al (10 s), Si (10 s), Ca (50 s) and Fe (50 s), and 50 nA for Mg (50 s), Ti (50 s), Mn (200 s), Cr (100 s), K (50 s), Cl (100 s) and S (50 s), and a defocused beam of 5 to 10 μm. Background counting times were 50 s for Cl and S. For olivines, the beam size was 1 μm and the beam current

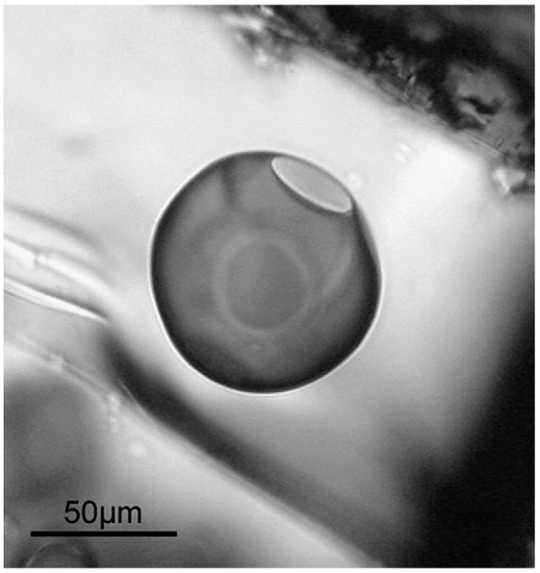

Fig. 1. Transmitted-light photomicrograph of a primary silicate melt inclusion in an olivine phenocryst from ARP73–10–03 MORB sample. Melt inclusions are glassy and often show a negative crystal morphology resulting from the minimization of interfacial energy: in this case, the equilibrium crystal shape is a rounded polyhedron with planar facets, as illustrated by the brighter facet in the upper right part of the inclusion.

was 15 nA for Si (10 s), Mg (10 s), Al (30 s) and Fe (50 s) and 50 nA for Ca (50 s) and Ni (50 s). The CAMECA set of standards (synthetic and natural minerals or oxides) was used for routine calibration, except for S which was calibrated on the basaltic glass standard ALV 981 R23 (Metrich and Clocchiatti, 1989; Metrich et al., 1991; Metrich and Clocchiatti, 1996). Analytical uncertainties were obtained from replicate measurements (Table S2, Supplementary data) of the natural glasses ALV 981 R23 (Metrich and Clocchiatti, 1989; Metrich et al., 1991; Metrich and Clocchiatti, 1996), USGS VG-2 (Dixon et al., 1991; Thordarson et al., 1996; de Hoog et al., 2001; Thornber et al., 2002), USGS VG-A99 (Dixon et al., 1991; Thordarson et al., 1996; de Hoog et al., 2001; Thornber et al., 2002), Ke12 (Palais and Sigurdsson, 1989; Metrich and Rutherford, 1992), Ve32 (Schiano et al., 1997) and ATHO (Oskarsson et al., 1982). The total analytical error, including both precision and accuracy of measurements, for the VG-2 basaltic glass was 2.1% rel. for SiO_2; 1.8% for MgO, TiO_2 and Al_2O_3; 2.4% for CaO; 2.7% for K_2O; 3.4% for FeO; 7–8% for Na_2O and P_2O_5; 12% for MnO and 50% for Cr_2O_3. Detection limits for S and Cl were ~75 and 50 ppm respectively and the total analytical error for S and Cl, including precision and accuracy of measurements, was 15% rel. for S and 40% rel. for Cl for the concentrations analyzed in our inclusions.

No effect of alkali-loss was observed on natural glasses of basaltic composition (ALV 981 R23, VG-2, VG-A99 and Ve32) under the analytical conditions applied during melt inclusion analysis: 15 kV, 8 nA and 10 µm beam. This effect exists under these conditions for Si-rich glasses only (Ke12 and ATHO).

3.2. Secondary ion mass spectrometry

Trace-element compositions were measured with a Cameca IMS 4f ion microprobe at CNR-IGG (Pavia). Gold-coated polished samples were bombarded by a mass-filtered $^{16}O^-$ primary beam accelerated at 12.5 kV. The primary ion beam had a current intensity ranging between 8 and 13 nA, which corresponds to a beam diameter <20 µm. The width of the energy slit was 50 eV and the voltage offset applied to the sample accelerating voltage (+4500 V) was −100 V. This corresponded to the analysis of secondary ions with emission kinetic energies in the range ~75–125 eV. The filtered secondary ions were extracted and focused under an ion image field of 25 µm. We used the largest contrast diaphragm and field aperture (diameters of 400- and 1800-µm, respectively), at a mass resolving power of ~600 (M/ΔM).

REE were analyzed with a procedure similar to that developed by Bottazzi et al. (1994) for silicates. La, Ce, Nd, Sm, Er and Yb were analysed by measuring the signals from one isotope, i.e. ^{139}La, ^{140}Ce, ^{146}Nd, ^{149}Sm, ^{167}Er and ^{174}Yb. For Eu we used a deconvolution procedure to remove BaO interferences from Eu isotopes. Ion signals were detected at mass 154, 160 and 162 in order to discriminate Gd (and Dy) from CeO and NdO interferences. Dy was monitored also through the isotope 163. Moreover, in the case of Er, we improved the reliability of analysis by evaluating the $^{151}Eu^{16}O$ contribution at mass 167 from the Eu^+ signal and from the oxidation ratio (i.e., EuO^+/Eu^+) as determined on the calibration standards under the adopted analytical conditions. A similar procedure was used to correct Yb from GdO interference at mass 174.

Concerning the other trace elements, signals were detected from the following isotopes: ^7Li, ^9Be, ^{11}B, ^{19}F, ^{39}K, ^{45}Sc, ^{47}Ti, ^{51}V, ^{52}Cr, ^{85}Rb, ^{88}Sr, ^{89}Y, ^{90}Zr, ^{93}Nb, ^{133}Cs and ^{137}Ba. All of them were monitored in the same analytical run together with the REE ion signals. There was a waiting time of 450 s necessary to obtain steady-state sputtering conditions, and then three acquisition cycles with the following counting times per cycle: Li (5 s), Be (5 s), B (10 s), F (10 s), Si (2 s), K (2 s), Sc (5 s), Ti (2 s), V (5 s), Cr (5 s), Rb (5 s), Sr (5 s), Y (10 s), Zr (8 s), Nb (8 s), Cs (8 s), Ba (8 s), La (10 s), Ce (10 s), Nd (10 s), Sm (15 s), Dy (20 s), Er and Yb (15 s

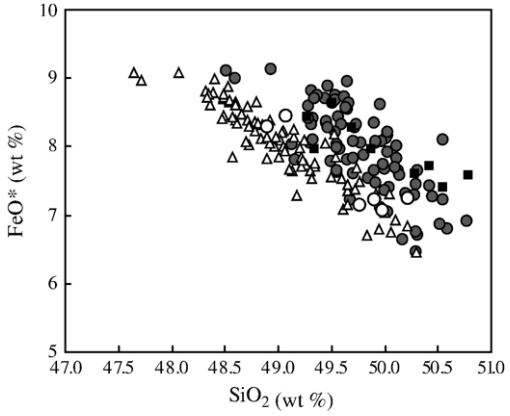

Fig. 2. FeO* vs SiO_2 concentrations for primitive olivine-hosted melt inclusions in ARP73–10–03 MORB. FeO* is total iron reported as FeO. Shaded circles correspond to the compositions of melt inclusions corrected for post-entrapment overgrowth of olivine, following the procedure described in Appendix A. Open circles correspond to the compositions of six melt inclusions homogenized with an optical heating stage. The compositions of melt inclusions normalized to the most primitive olivine $Fo_{91.3}$ (open triangles; i.e., compositions are brought back to a Mg# value of 0.78, which corresponds to the composition of a melt in equilibrium with $Fo_{91.3}$ olivine, by dissolving olivine into the melt) are also reported for comparison. The correlation is still valid in the "normalized" compositions, indicating that pre-entrapment crystallization of olivine cannot produce the compositional variation of the melt inclusions. Melt inclusions trapped in spinel crystals from the same sample (solid squares, Kamenetsky, 1996) display chemical compositions similar to olivine melt inclusions from this study.

each). For the deconvolution procedure the counting times were: 10 s (mass 151), 5 s (mass 154), 20 s (mass 160 and 162, each). The instrumental background was tested at mass 1.5 amu and resulted in a negligible contribution. $^{30}Si^{+}$ was selected as the isotope of the reference element (Si) for these matrices.

Mass calibration of the ion signals in the magnet of the ion microprobe was realized with the international standard SRM-NIST 610. Seven well-characterized reference silicate standards (371, 315, 370, KSS, JDF-D2, BB and BCR-2G; Table S3, Supplementary data) were used to convert ion intensities into elemental concentrations. NIST 610 was used as the primary standard for B (Ottolini et al., 1993), whereas Li and Be were calibrated with basalt BB, kaersutite Soda Springs (KSS) and glass BCR-2G. F was calibrated via KSS which belongs to our working curve defined for F in silicates: uncertainty by ~20% rel. (see Ottolini et al., 1994 for further details).

Comparison between the SIMS concentrations in the standards and the reference values, together with the precision (1σ) that represents the reproducibility on three analytical sessions over a one-month span can be found as supplementary information (Table S3, Supplementary data). Relative precision is generally better than 10% for all the elements. The precision of a single analysis from Poisson counting statistics for the various isotopes detected is on the order of 10% or better at ppm wt concentration (see Messiga et al., 1995 for further details). Corrections were done to remove residual interferences at mass 45 (amu) for Sc ($^{29}Si^{16}O^{+}$) and mass 52 (amu) for Cr ($^{24}Mg^{28}Si^{+}$). The trace-element concentrations were derived from the SiO_2 (wt.%) values from EMP analyses in the melt inclusions. The agreement between the reference and SIMS data (accuracy) is generally within the uncertainty of analysis ($1–2\sigma$). Larger scatter was obtained for the alkali elements Rb and Cs which are very mobile under the O^{-} primary beam. In the case of Rb, the glasses 315, 371 and 370 were used as primary standards since their Rb concentration is on the same order of that in the melt inclusions. Considering the overall uncertainty of the reference data for Rb and Cs in the standards used in this study, we can estimate an uncertainty of ≤20–25% rel. in the final SIMS data. Since the data for K assumed as the reference for SIMS are generally derived from electron microprobe analysis and bias in EMPA measurement was revealed as a consequence of alkali-loss under the electron beam, the accuracy for K was ≤15% rel. Similar accuracy (≤15% rel.) is estimated for Cr.

4. Results

Major- and trace-element compositions of the melt inclusions, after correction for post-entrapment crystallization of the host phase (see below), are presented in Table S1 in supplementary data.

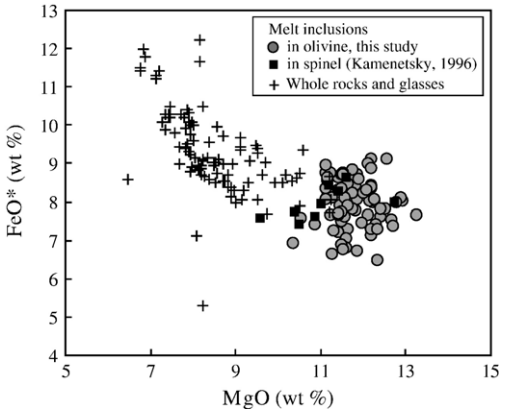

Fig. 3. FeO* vs MgO plot of olivine-hosted (this study) and spinel-hosted (Kamenetsky, 1996) melt inclusions from the ARP73–10–03 sample, FAMOUS whole rocks and basalt glasses (Langmuir et al., 1977; Bryan, 1979; Le Roex et al., 1981). Melt inclusions plot at the primitive end of FAMOUS basalt trends. Two whole rock compositions with MgO>15 wt.% have been omitted for clarity.

4.1. Major-element compositions

At the time of entrapment, the melt is in thermodynamic equilibrium with the crystallizing host olivine. During cooling of the system, olivine crystallization occurs at the inclusion walls, which modifies the melt composition. Consequently, the Mg–Fe exchange coefficient $K_{DOl-Liq}^{Fe-Mg} = \frac{X_{Liq}^{Mg}/X_{Ol}^{Mg}}{X_{Liq}^{Fe^{2+}}/X_{Ol}^{Fe^{2+}}}$ between inclusions (Liq) and their host olivines (Ol) decreases to values much lower (between 0.13 and 0.20) than the nominal value of 0.30±0.03 generally admitted for basaltic magmas at 1 atm (Roeder and Emslie, 1970). Correction for this post-entrapment overgrowth was carried out numerically as explained in Appendix A. This was done by using the model for $K_{DOl-Liq}^{Fe-Mg}$ recently proposed by Toplis (2005), which quantifies the effects of pressure, temperature, olivine and liquid compositions on the exchange coefficient. For comparison with the corrected data, the initial major-element

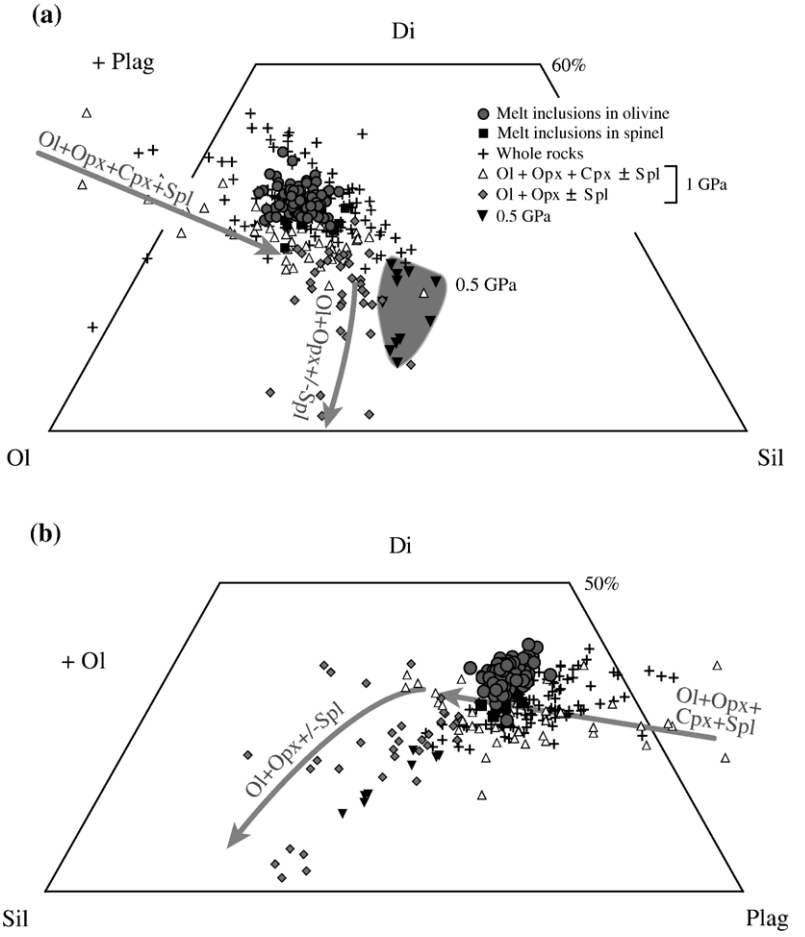

Fig. 4. Ternary projections of the major-element compositions of olivine-hosted (this study) and spinel-hosted (Kamenetsky, 1996) melt inclusions, and experimental lherzolite melts into the normative tetrahedron olivine-clinopyroxene-plagioclase-silica using the projection scheme of Walker et al. (1979). Compositions of melt inclusions in olivine are corrected for post-entrapment olivine growth, or homogenized. Experimental peridotite melts at 1 GPa (Baker et al., 1995; Hirschmann et al., 1998; Pickering-Witter and Johnston, 2000; Falloon et al., 2001; Schwab and Johnston, 2001; Wasylenki et al., 2003; Laporte et al., 2004) are divided in two groups: 1) melts in equilibrium with olivine+orthopyroxene+clinopyroxene±spinel (arrow Ol+Opx+Cpx±Spl, which points toward increasing extents of melting); and 2) compositions in equilibrium with olivine+orthopyroxene± spinel (arrow Ol+Opx±Spl). Experimental melts produced at 0.5 GPa from a plagioclase/spinel peridotite (D. Laporte, unpublished data) are also shown to indicate that the compositional variations in the melt inclusions are not primarily controlled by variation in the depth of melting. Whole rock data from the FAMOUS zone (Langmuir et al., 1977; Bryan, 1979; Le Roex et al., 1981; crosses) have also been reported for comparison. Melt compositions are projected from plagioclase onto the olivine–silica–diopside plane (a) and from olivine onto the plagioclase–diopside–silica plane (b). In (a), experimental melts produced at higher pressures (up to 3 GPa; Kushiro, 1996) would plot closer to the olivine apex and are therefore inconsistent with the melt inclusion data. In (a) and (b), melt inclusions are enriched in the diopside component compared to experimental and most whole rock data. This enrichment cannot be due to olivine crystallization prior to melt entrapment as projection (b) is not sensitive to olivine fractionation.

compositions of six glassy melt inclusions were experimentally restored by heating up to the homogenization temperature (1270–1300 °C) using a high temperature, He-atmosphere, optically controlled heating/quenching stage. Compositions of the heated inclusions plot along the trends of numerically corrected compositions (Fig. 2).

It has been proposed (Danyushevsky et al., 2000; Gaetani and Watson, 2000, 2002) that major-element compositions of melt inclusions trapped in olivine could be modified after entrapment by the combined effects of Fe–Mg exchange with the host crystal and diffusive re-equilibration with the external melt. The result is a significant decrease in FeO and increase in MgO in the trapped melt. Major-element compositions of the melt inclusions fall at the primitive end of the trend of whole rocks and basaltic glasses from the same area, and no evidence for "FeO-loss" is observed (Fig. 3). Another argument against significant re-equilibration of the inclusions is the consistency between their major-element compositions (including FeO) and those of inclusions hosted in spinel (Kamenetsky, 1996; Figs. 2 and 3).

After correction for post-entrapment crystallization, or using experimentally heated samples, silicate melt inclusions in high-Mg host olivines ($Fo_{87.2}$ to $Fo_{91.3}$) display Mg#s ($Mg/(Mg+Fe^{2+})$) ranging from 0.70 to 0.78. When projected from plagioclase onto the olivine-silica-diopside plane (Walker et al., 1979; Stolper, 1980), they plot close to experimental peridotite melts produced at 1 GPa (Baker et al., 1995; Hirschmann et al., 1998; Pickering-Witter and Johnston, 2000; Falloon et al., 2001; Schwab and Johnston, 2001; Wasylenki et al., 2003; Laporte et al., 2004), which confirms their near-primary characteristic (Fig. 4a). However, they show a slight enrichment in the diopside component. This enrichment cannot be solely due to a pre-entrapment olivine fractionation process as it is also observed in the projection from olivine onto the silica-diopside-plagioclase plane (Fig. 4b). Plausible causes for this enrichment will be evaluated in Section 5.1.

The inclusions have olivine tholeiite compositions consistent with previous studies (Kamenetsky, 1996; Shimizu, 1998). They display significant variations in major-elements (e.g., 6.5–9.1 wt.% FeO*, 10.4–13.3 wt.% MgO, 1.25–1.85 wt.% Na_2O) and define clear correlations in binary diagrams (Fig. 2). Such variations were already present in the data set before correction for host olivine crystallization, so they cannot be an artifact of the correction procedure. It is important to note that although melt inclusions plot at the primitive end of the compositional trend of FAMOUS whole rocks (Fig. 3), the major-element correlations defined in the inclusions are distinct from the whole rock trends. This observation is consistent with the assumption that melt inclusions in early-formed minerals record early steps in the evolution

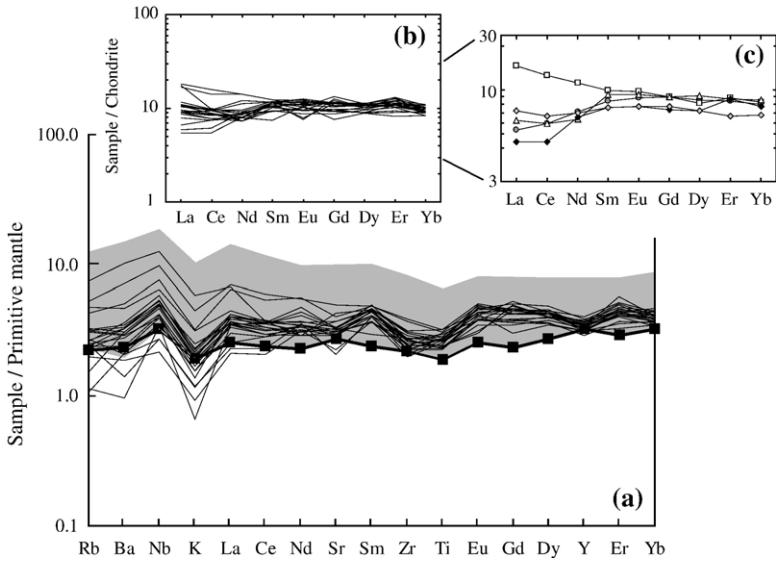

Fig. 5. Primitive mantle-normalized diagram (Sun and McDonough, 1989) (a) showing trace-element data for olivine-hosted melt inclusions in MORB sample ARP73–10–03. The elements are classified according to the incompatibility sequence previously determined for MORB genesis (Hofmann, 1988). Also shown for comparison are the compositions of FAMOUS whole rocks and basalt glasses (shaded area; Langmuir et al., 1977; White and Bryan, 1977; Le Roex et al., 1981) and the composition of the sample ARP73–10–03 used for this study (solid squares). The insert (b) shows the chondrite C1- (Sun and McDonough, 1989) normalized abundance patterns for rare-earth elements in the melt inclusions. Crossing of REE patterns in the melt inclusion data is illustrated by five representative compositions (c).

of magmas before aggregation at shallower levels (Sobolev, 1996; Shimizu, 1998; Schiano, 2003). Also, as illustrated in Fig. 2, progressive pre-entrapment crystallization of olivine (from $Fo_{91.3}$ to $Fo_{87.2}$; i.e., the whole range of composition of the host olivines) cannot produce the compositional variation of the melt inclusions, although it might be responsible for some of the scatter observed within the correlations. These results unambiguously demonstrate that primitive magmas with significantly different major-element compositions coexisted at the site of olivine crystallization and melt entrapment.

4.2. Trace-element compositions

The main features of the REE patterns on a chondrite-normalized plot are the presence of both LREE-enriched and LREE-depleted patterns and the lack of correlation between HREE abundances and the degree of LREE enrichment, as expressed by the crossing of REE patterns (Fig. 5). In detail, while most inclusions have very similar REE patterns with nearly flat shapes, four LREE-enriched inclusions have $(La/Sm)_N$ ratios >1.2, while four LREE-depleted inclusions show $(La/Sm)_N$ ratios <0.75. The compositional range of the trapped melts within one sample is almost as large as the whole range found in bulk rocks and basaltic glasses from the FAMOUS zone (Langmuir et al., 1977; White and Bryan, 1977; Le Roex et al., 1981; Fig. 5) and the range of incompatible-elements overlaps for the most part the field of N-type MORB. In detail, however, variation of the moderately incompatible-elements is larger for whole rocks than for melt inclusions while the range of variation for the most incompatible-elements (Rb, Ba, Nb and K) is similar (Fig. 5).

4.3. Major and trace-element heterogeneity and decoupling

The variations in the major-element concentrations (standard deviation/mean concentration) in the melt inclusions are greater for TiO_2 (12%), Na_2O (9%) and

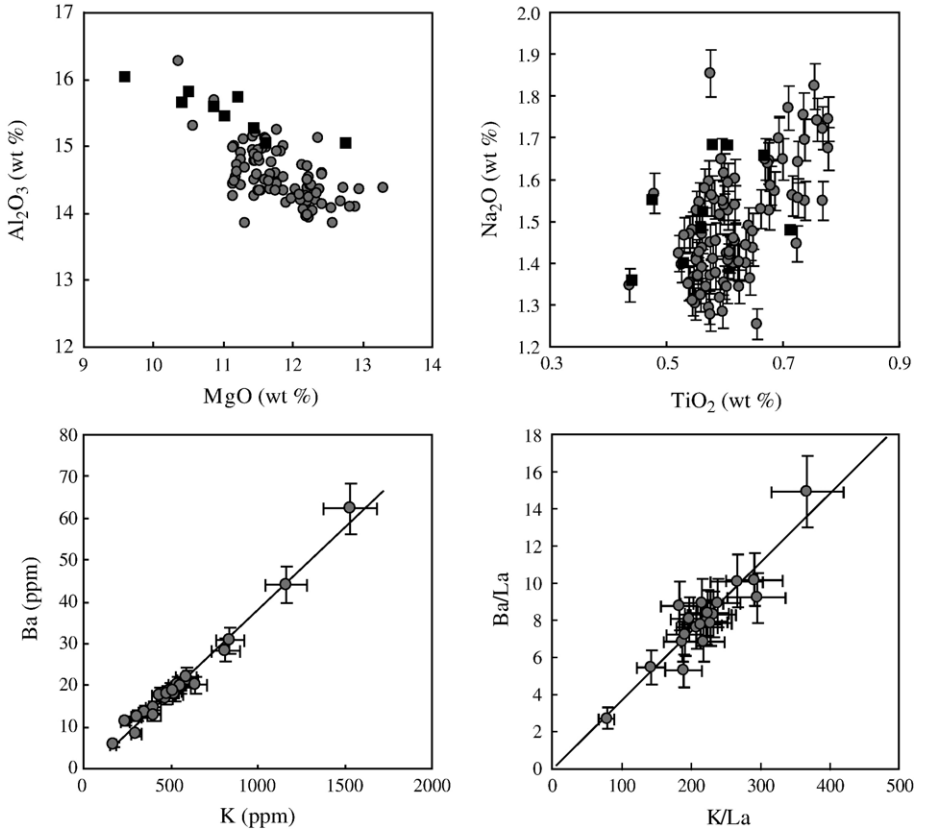

Fig. 6. Major and trace-element trends in melt inclusions. Solid squares are melt inclusions trapped in spinel (Kamenetsky, 1996). The chemical heterogeneity defines binary trends for both major and trace elements between an "enriched" end-member (high Al_2O_3, TiO_2 and Na_2O, and low MgO for major-elements; high Ba and K for trace elements) and a depleted end-member. 2 σ errors are indicated when larger than the size of the symbols.

FeO (8%) than for other elements (also observed in melt inclusions trapped within spinels; Kamenetsky, 1996). The major-element compositions define binary trends (Figs. 2 and 6 and see Appendix B) between an enriched end-member characterized by high FeO, Na_2O, TiO_2, Al_2O_3, and relatively low SiO_2 and MgO contents, and a depleted end-member characterized by low FeO, Na_2O, TiO_2, Al_2O_3, and high SiO_2 and MgO contents. Trace-element heterogeneity also defines binary trends in element–element plots, ratio–element plots and ratio–ratio plots (Fig. 6 and Appendix B) between an end-member enriched essentially in the most incompatible-elements (e.g., Rb, Ba, K, Nb) and a depleted one.

An important feature of the chemical compositions of the melt inclusions is the apparent decoupling between major- and trace-element concentrations; i.e., no correlation between major- and trace-element concentrations is observed (see Appendix B). This characteristic has also been pointed out for whole rocks from the FAMOUS region (Langmuir et al., 1977; Bryan, 1979) and seems inconsistent with a single simple petrogenetic process. These observations will be a key point of the following discussion.

5. Discussion

Melt inclusions trapped in Mg-rich olivine crystals from the ARP73–10–03 MORB display a large range of major- and trace-element compositions and show chemical trends in binary diagrams (Fig. 6), suggesting that they constitute a suite of genetically-related primitive magmas. Various processes could have produced this evolution, including progressive partial melting, mantle-melt interaction during melt transport and/or mixing between different mantle sources. In the following, these models are discussed and evaluated in the light of the results summarized above.

5.1. CaO content in the melt inclusions

The olivine-hosted melt inclusions have higher CaO/Al_2O_3 ratios (up to 1) than most FAMOUS whole rocks (Langmuir et al., 1977; Bryan, 1979; Le Roex et al., 1981) and spinel-hosted melt inclusions (Fig. 7; Kamenetsky, 1996). In addition, their CaO content extends to values (up to 14.1 wt.%) higher than those reached during experimental lherzolite melting under dry or hydrous conditions (see discussion in Schiano et al., 2000; Médard et al., 2004). An early episode of olivine fractionation at high pressure could account for the high CaO contents of the melt inclusions, but not for their high CaO/Al_2O_3 ratios.

The presence in some MORB of olivine-hosted melt inclusions with high CaO contents, sometimes associated with positive Sr anomalies and/or high Al_2O_3 contents (Kamenetsky and Crawford, 1998; Danyushevsky et al., 2004) has been interpreted as reflecting reactions between

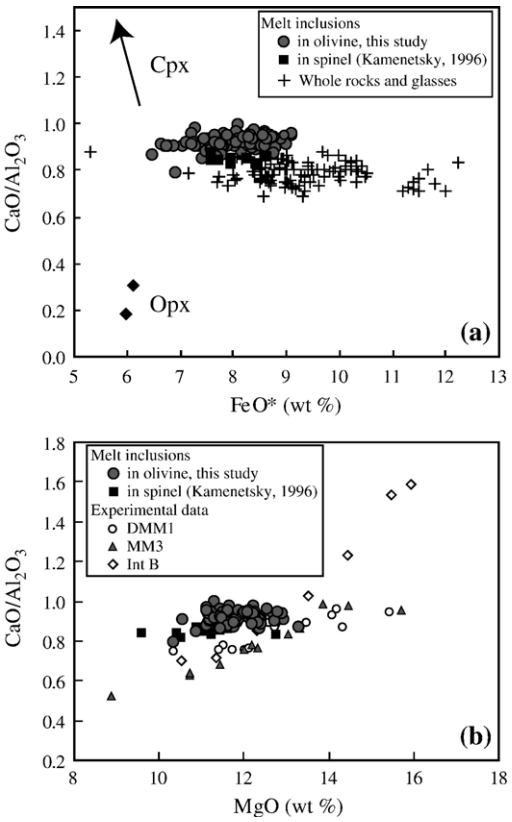

Fig. 7. Variation of CaO/Al_2O_3 as a function of FeO* (a) and MgO (b). Shaded circles are melt inclusions in olivine (this study). Solid squares are melt inclusions in spinel from the same sample (Kamenetsky, 1996). (a) Solid diamonds are orthopyroxenes selected from experimental starting materials (Wasylenki et al., 2003; Laporte et al., 2004); clinopyroxenes with elevated CaO/Al_2O_3 values are represented by the arrow. Whole rock and glasses data from the FAMOUS zone (Langmuir et al., 1977; Bryan, 1979; Le Roex et al., 1981; crosses) have also been reported for comparison. No evidence of pyroxene dissolution is observed from this diagram. (b) Experimental melts from model refractory lherzolite DMM1 (Wasylenki et al., 2003) and fertile lherzolite MM3 (Baker et al., 1995) and the olivine+clinopyroxene-rich mix INT-B (Schwab and Johnston, 2001) are reported. CaO/Al_2O_3 ratio is equal to 0.9 for DMM1 and MM3, and 3.4 for INT-B. This figure shows that at high MgO contents (13.5–16 wt.%), pyroxenite or wehrlite melting produces CaO/Al_2O_3 ratios that are much too high, while peridotite melting can account for the values of CaO/Al_2O_3 ratio in the melt inclusions. Melt inclusions in Cr-spinel analyzed by Kamenetsky (1996) in the ARP73–10–03 sample (solid squares) have similar mean compositions to those in olivines, but some display slightly lower MgO contents and CaO/Al_2O_3 ratios, which may indicate that they contain lower degree melts than the inclusions in olivines.

plagioclase and/or clinopyroxene and primitive mantle melts. However, no Sr anomalies are observed in the FAMOUS melt inclusions, which rules out the hypothesis of plagioclase assimilation. Also, dissolution of clinopyroxene by interaction of ascending melts with wehrlites or crustal gabbros results in the formation of Cr-rich spinel (Cr# up to 70 mol%, instead of <60 mol% in MORB) and melts characterized by high CaO and low Al_2O_3 (~12 wt.%) (Kamenetsky and Crawford, 1998). In contrast, the FAMOUS melt inclusions display "normal" Al_2O_3 contents (13.9–16.3 wt.%) and the Cr# of spinels from the host rock does not exceed 53 mol% (Kamenetsky, 1996). Finally, a plot of CaO/Al_2O_3 vs FeO* (Fig. 7a) shows no evidence for clinopyroxene or orthopyroxene dissolution.

An alternative explanation is that the CaO-rich compositions of the inclusions partially reflect combined dissolution-reaction-mixing processes due to localized fast crystallization rates at the margins of the "plumbing" system (Danyushevsky et al., 2004). Following this hypothesis, high cooling rates would enhance rapid crystallization of olivines containing large melt inclusions that sample the reaction zone. However, the ARP73–10–03 melt inclusions are found in olivine phenocrysts that display a polyhedral habit, a morphology which typically forms during slow crystal growth (Baronnet, 1984), and therefore can hardly be reconciled with high cooling rates.

Post-entrapment re-equilibration of melt inclusions with the surrounding melt by diffusion of Mg, Fe and Ca through the host crystal can also play a role in generating CaO-rich inclusions (Gaetani et al., 2002). However, as Fe and Mg interdiffusion rates in olivine are faster than Ca diffusion (Jurewicz and Watson, 1988), FeO and MgO contents should re-equilibrate before CaO. As previously discussed, no evidence for diffusive Mg–Fe re-equilibration was found in our melt inclusions.

Fig. 4b shows that the melt inclusions are enriched in the diopside component (i.e., characterized by high CaO contents and CaO/Al_2O_3 ratios) rather than simply characterized by high CaO concentrations. During melting, the diopside content of lherzolite melts increases until clinopyroxene is exhausted from the residue. In addition, experimental studies of peridotite melting indicate that the diopside component in melt compositions increases with increasing CaO/Al_2O_3 ratio in the source (Fig. 7b). Melts with high CaO/Al_2O_3 ratios could thus result from melting of highly depleted lherzolites with a very low fraction of clinopyroxene (Wasylenki et al., 2003), but also from high degrees of melting of fertile lherzolites (Baker et al., 1995). However, partial melts of refractory lherzolites or high-degree melts of fertile lherzolites display elevated MgO contents (≥14 wt.%), requiring olivine fractionation to decrease their MgO contents to those of the FAMOUS melt inclusions (10.4–13.3 wt.%). In this case, the maximum CaO content in the primary lherzolite melts is increased to the maximum value in the melt inclusions by olivine crystallization. Accordingly, the CaO contents and CaO/Al_2O_3 ratios (the latter being unmodified by olivine fractionation) in the melt inclusions can be successfully reproduced by partial melting of refractory or fertile lherzolites with high CaO/Al_2O_3 ratios (Fig. 7b). Melting of clinopyroxene-enriched and orthopyroxene-depleted lithologies such as wehrlites or garnet pyroxenites is therefore not required.

5.2. The role of melt–mantle interaction

Magmas migrating through the mantle can interact chemically with the matrix towards a state of equilibrium (Navon and Stolper, 1987). Several studies have thus emphasized the role of reactive melt transport on the geochemical features of magmas (McKenzie, 1984; Spiegelman and Elliot, 1993; Kelemen et al., 1995a,b; Spiegelman et al., 2001; Spiegelman and Kelemen, 2003). For instance, dunite channels observed in mantle sections of ophiolite and peridotite massifs have been interpreted as the results of reactive dissolution as magmas percolate through a lherzolite or harzburgite mantle towards the surface (Kelemen et al., 1995a,b, 1997; Asimow and Stolper, 1999).

In a previous study of olivine-hosted melt inclusions in another basalt from the FAMOUS area, Shimizu (1998) suggested that geochemical variations in the melts resulted from interaction with wall-rock mantle, according to a combined assimilation-fractional crystallization (AFC) mechanism (DePaolo, 1981). Zone refining or AFC models focus on trace-element effects at the melt front and thus do not provide direct information on the temporal evolution of melts emerging from the matrix column through which magma flows. Therefore we have used the model of equilibrium reactive transport in the mantle described by Reiners (1998) to evaluate whether melt/matrix interaction could have played a role in the generation of the melts trapped in the FAMOUS inclusions. In this model, melt migrates through the column of reactive mantle, successive melt batches emerge and their compositional variations reflect the reactive capacity of the mantle (see caption of Fig. 8 for model parameters).

In our calculations the source and the column matrix are similar in composition, so the melt and the solid will be respectively enriched and depleted in incompatible elements during the exchange mechanism. Chemical

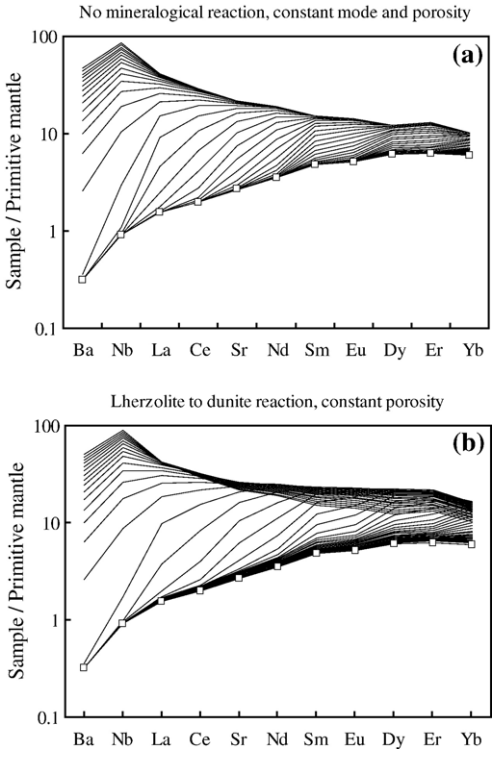

Fig. 8. Primitive mantle-normalized diagram (Sun and McDonough, 1989) showing trace-element evolution of model melts emerging from a mantle column and produced by chemical interaction with the mantle matrix during melt transport as described by Reiners (1998). The model assumes local trace-element equilibrium between migrating melt and surrounding mantle. The initial melt introduced at the base of the mantle column (squares) is produced by 5% continuous melting (Sobolev and Shimizu, 1993b) of a depleted MORB mantle source ("average" DMM of Workman and Hart, 2005). Trace-element patterns are shown for melts emerging at different times: from the melt front composition (the first melt that emerges from the column, and thus the most enriched one) until the return to the input melt composition. In our calculation, the same spinel lherzolite composition is used to simulate the melt source and the column matrix. The initial porosity of the matrix is 5% since intergranular porosity in the mantle ranges between 1 and 6.5% (Kelemen et al., 1997). In our calculations, chemical interaction occurs either with no mineralogical reaction in the matrix (a) or with a lherzolite-to-dunite reaction by dissolution of pyroxene (b). Porosity is maintained at a constant percentage in the calculations presented in these figures (5%), but the effect of porosity changes on melt compositions is small compared to the effects of mineralogical reactions.

interaction occurs in two different manners: (i) no mineralogical reaction in the matrix, and (ii) lherzolite-to-dunite reaction by dissolution of pyroxene. As demonstrated by Reiners (1998) and also observed in our calculations (Fig. 8), the main features of reactive melt transport are: (1) enrichment of incompatible-elements in the leading melt batches and decreasing concentrations in successive melts (i.e., with time), (2) chromatographic decoupling in the variation of trace-element compositions (i.e., decoupling of concentrations of trace elements with different bulk partition coefficients in successive melt batches emerging at the top of the column), (3) large variation in HREE in the case of lherzolite-to-dunite reaction in the column.

No significant HREE variations are found in the inclusion data contrary to what is observed in the case of lherzolite-to-dunite reaction (Figs. 5 and 8). Moreover, in the model with no mineralogical reaction, the chromatographic decoupling of concentrations of trace elements with varying bulk partition coefficients in successive melt batches emerging from the column is not related to a crossing of the patterns, contrary to what is observed in the melt inclusions. This suggests that the trace-element variation in the FAMOUS inclusions is dominated mainly by melting processes, mixing of melts and/or source heterogeneity rather than reactive melt transport.

5.3. The role of partial melting processes

In this section, we assess whether variable extents of partial melting could be a plausible explanation for the evolution of the major- and trace-element compositions of the melt inclusions. We test this hypothesis using different models of partial melting, including isobaric versus polybaric melting processes. The models are based on calculations from the latest version of the pHMELTS algorithm, Adiabat_1ph (Smith and Asimow, 2005), and the ridge model of Langmuir et al. (1992).

MELTS computational algorithm applies thermodynamic models of minerals and silicate liquids to calculate phase equilibria as a function of intensive variables and bulk composition (Ghiorso and Sack, 1995). New calibrations and refinements have been incorporated in a revised version, pMELTS (Ghiorso et al., 2002), which has been expanded again recently to the pHMELTS model that includes H_2O and trace elements (Asimow et al., 2004; Smith and Asimow, 2005). Given the discrepancies that exist between pHMELTS calculations and the results of peridotite melting experiments (Ghiorso et al., 2002), we focus on comparing calculated trends with the melt inclusion evolution rather than using them to predict accurate quantitative values.

5.3.1. Isobaric partial melting

Two types of melting regime were investigated using pHMELTS: batch and continuous melting. During batch melting, melt remains in contact with the residue and re-equilibrates at every temperature. During continuous melting, melt is continuously extracted from the mantle except a small fraction (2 wt.% in this study) which is

retained in the residue. The coherency for major-elements between the batch melting calculations and experimental melts of lherzolite rock-types at 1 GPa (Baker et al., 1995; Kushiro, 1996; Hirschmann et al., 1998; Wasylenki et al., 2003; Laporte et al., 2004) is illustrated in Fig. 9. Experimental melts of MM3 fertile lherzolite (Baker et al., 1995; Hirschmann et al., 1998) are consistent with isobaric batch trends calculated with pHMELTS, despite a slight MgO overestimation and Al_2O_3 and CaO underestimation in the model melts.

Overall, major-element compositions of the inclusions are consistent with 1 GPa batch melts formed either at high melt fractions (up to 25%) from a fertile lherzolite or

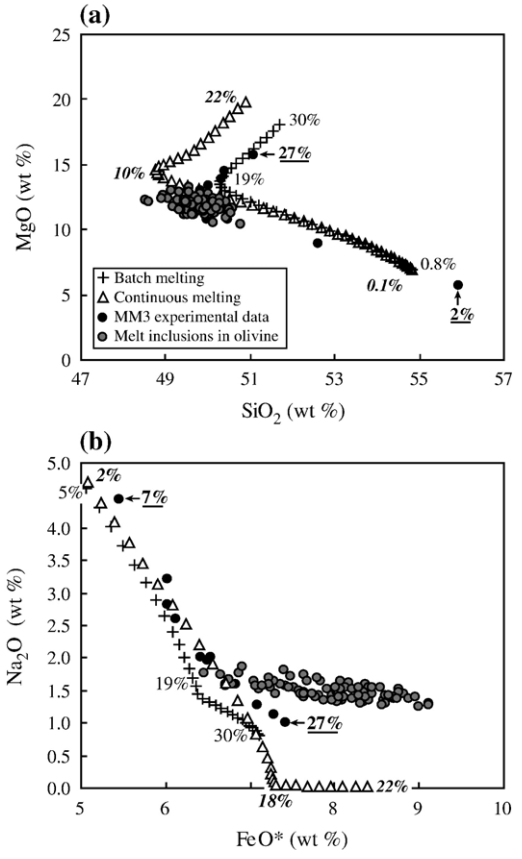

Fig. 9. MgO vs SiO_2 (a) and Na_2O vs FeO* (b) in olivine-hosted melt inclusions (shaded circles) and experimental melts produced by melting of MM3 starting composition at 1 GPa (solid circles; Baker et al., 1995; Hirschmann et al., 1998). Crosses and triangles are pHMELTS model melts for isobaric batch and continuous melting, respectively, at 1 GPa. Degrees of melting are indicated along the curves with a regular font for batch melts, italic for continuous melts and bold underlined for experimental melts. Oxygen fugacity is set at QFM-1 in the calculations. In the continuous melting model, 2% of melt is retained in the source. It should be noted that the range of the degree of melting that could account for the variation in the melt inclusions differs from one element to another.

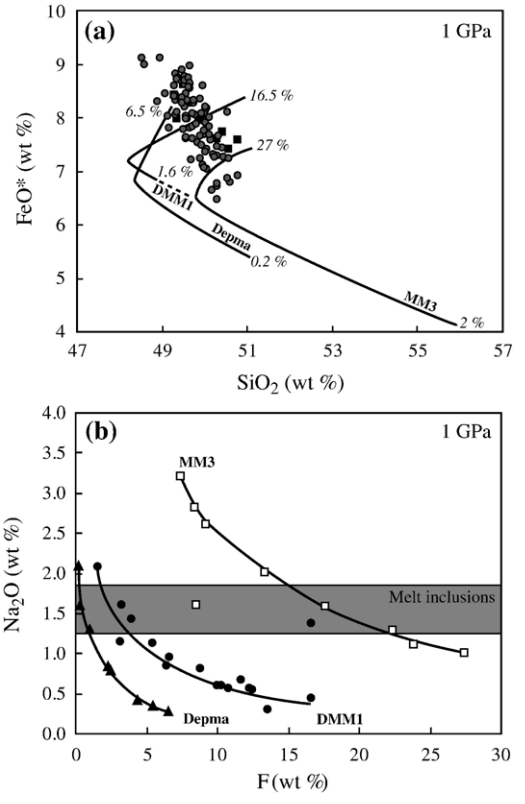

Fig. 10. (a) FeO* vs SiO_2 in olivine-hosted melt inclusions (this study; shaded circles) and spinel-hosted melt inclusions (solid squares; Kamenetsky, 1996) from MORB ARP73–10–03. Melt fractions (wt. %) are reported along the trends. (b) Na_2O in experimental lherzolite melts vs degree of melting, F. Experimental melting trends at 1 GPa are from the following starting materials: MM3 (Baker et al., 1995) fertile lherzolite and DMM1 (Wasylenki et al., 2003) and Depma (Laporte et al., 2004) harzburgites. Black curves correspond to the best fits of experimental melting trends. The range of Na_2O contents in the melt inclusions is represented by the shaded area.

at low melt fractions (1–5%) from a refractory lherzolite (Fig. 10). However, some inconsistencies remain such as the relatively high FeO* contents in the melt inclusions compared to experimental melts produced at 1 GPa (Fig. 10a) and the small variation in the Na_2O content (Fig. 10b). Furthermore the degree of melting necessary to account for the concentration range strongly differs from one element to the other (Fig. 10). For instance, FeO concentrations require a much larger range of the degree of melting than other elements, in particular for a refractory lherzolite source (Fig. 10a). These observations rule out a major role of isobaric melting in the evolution of the compositions of the melt inclusions.

5.3.2. Polybaric partial melting

Polybaric, isentropic melting of the upwelling mantle, where instantaneous melts are produced over a range of

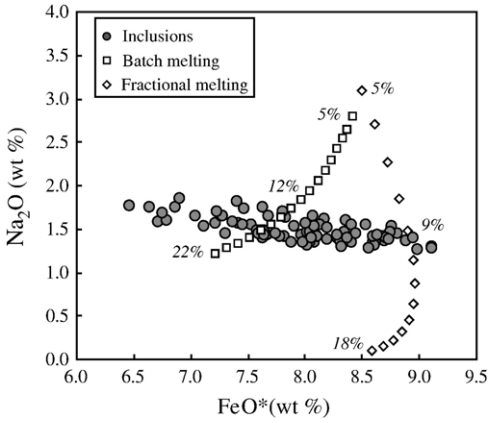

Fig. 11. Evolution of instantaneous melts computed using the ridge melting model of Langmuir et al. (1992), over a range of pressures of ~2.7–0.5 GPa. Squares and diamonds correspond to batch and fractional melting trends, respectively; melt fractions (wt.%) are indicated along the curves. Source composition used in the calculations is the average DMM from Workman and Hart (2005) (Table 1). Melt inclusions show a large variation in FeO* correlated with a small decrease of the abundance of incompatible-elements such as NaO_2 (also true for TiO_2), while polybaric melting predicts larger variations of Na_2O with the melt fraction.

pressures from the garnet to the plagioclase stability fields and subsequently mixed, is generally thought to be a more viable process than isobaric melting to explain MORB petrogenesis and abyssal peridotite compositions (Johnson et al., 1990; Langmuir et al., 1992). Therefore we have applied models of isentropic melting in the pressure range 4–0.4 GPa in an attempt to reproduce the melt inclusion compositions. We used two models of MORB production based on empirical parameterization (Langmuir et al., 1992; C.H. Langmuir, personal communication) and thermodynamic principles (pHMELTS, Smith and Asimow, 2005), respectively (see captions of Figs. 11 and 12 for model parameters).

In our calculations with the ridge model of Langmuir et al. (1992), the adiabatically ascending mantle material intersects its solidus at a temperature of 1400 °C, which corresponds to a pressure of initial melting of ~2.7 GPa for the composition of the average DMM from Workman and Hart (2005) (Table 1). Partition coefficients for major-elements change with pressure and temperature, therefore the concentrations were calculated incrementally at each 0.1 GPa pressure step in a process of batch or fractional melting. Instantaneous melts, rather than aggregated melts, were retained from these calculations, because melt inclusions are likely to sample different batches extracted at various pressures rather than pooled melts at the top of the melting regime.

Although both the ridge model of Langmuir et al. (1992) and the polybaric melting calculations with pHMELTS can account for most major-element variations in the melt inclusions by continuous isentropic melting, they fail to reproduce some of the observed correlations, in particular Na_2O vs FeO* (Figs. 11 and 12). Our observations thus suggest that polybaric melting cannot provide a unique solution to the petrogenetic problems raised by the melt inclusion compositions.

Most major-element evolutions of the melt inclusions differ from the trends of the whole rocks from the FAMOUS zone (Fig. 12), but are consistent with the global trends defined for MORB by Klein and Langmuir (1987) for normal ridges. The global trends have been interpreted in terms of temperature variation in the mantle and could correspond to pooled melts produced in different melting regimes for different pressures of intersection of the mantle solidus (Klein and Langmuir, 1987). Accordingly, the melt inclusion correlations that cannot simply be accounted for by a simple process of polybaric melting (for example, Na_2O vs FeO*, Fig. 12) could reflect mixing of instantaneous melts produced in melting regimes characterized by different potential temperatures and/or water contents (Fig. 12). However, this interpretation proposed for the large-scale MORB variability seems unrealistic at the scale of a single sample as it would imply a large range of temperature

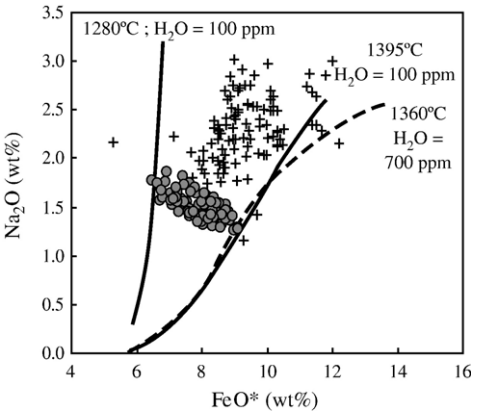

Fig. 12. Na_2O vs FeO* in olivine-hosted melt inclusions (circles), whole rocks from the FAMOUS zone (crosses) and pHMELTS model liquids. Isentropic continuous melting of the average DMM composition (Table 1; Workman and Hart, 2005) is modeled at different potential mantle temperatures (1280, 1360 and 1395 °C) and with various H_2O contents in the source ranging between 100 ppm (solid curves) and 700 ppm (dashed curve). Mixing of batches extracted from different melting regimes characterized by various potential temperatures in the range 1280–1395 °C or 1280–1360 °C in the case of H_2O addition in the source could account for the variability in FeO* in the melt inclusions.

Table 1
Fitted source composition for the melting models compared to the DMM composition from Workman and Hart (2005)

	Workman and Hart (2005)	Fitted composition
SiO_2 (wt.%)	44.71	44.71
Al_2O_3	3.98	3.98
Fe_2O_3	0.191	0.191
FeO	8.008	8.008
MnO	0.13	0.13
MgO	38.73	38.73
CaO	3.17	3.17
Na_2O	0.13	0.28
Cr_2O_3	0.57	0.57
TiO_2	0.13	0.13
Rb (ppm)	0.05	0.15
Ba	0.563	2.2
Nb	0.1485	0.35
La	0.192	0.27
Ce	0.55	0.6
Nd	0.581	0.57
Sr	7.664	6.3
Sm	0.239	0.2
Zr	5.082	3
Ti	716.3	450
Eu	0.096	0.075
Gd	0.358	0.3
Dy	0.505	0.35
Y	3.328	1.8
Er	0.348	0.25
Yb	0.365	0.25
H_2O		100

over short distances: 1280–1395 °C (Fig. 12) for a DMM source composition (Workman and Hart, 2005) and 1345–1620 °C for a MM3 fertile source composition (Baker et al., 1995). It should be noted, however, that the required range of the mantle temperature is reduced to 1280–1360 °C for DMM melting if the H_2O content in the source varies between ~100 and 700 ppm (Fig. 12), as proposed on a larger scale for the FAZAR MORB samples near the Azores (Asimow et al., 2004).

In an attempt to reproduce the trace-element compositions of the melt inclusions by a model of polybaric melting, we also performed the different pHMELTS calculations described above for trace elements. The trace-element composition of the source has been adjusted from the composition of the average DMM (Workman and Hart, 2005) in order to reproduce most of the features in the melt inclusion data. The best fit was obtained for a source which is enriched in the very incompatible-elements such as Rb, Ba, Nb and La (Table 1) in comparison with the DMM composition (Workman and Hart, 2005). On the contrary, contents of M- and HREE and Ti and Zr must be depleted in the source to reproduce the melt inclusion data. The changes in mineral proportions in the source during melting are taken into account in the calculations with pHMELTS (Asimow et al., 2004; Smith and Asimow, 2005). Mineral/melt partition coefficients used in the calculations are reported in Appendix C. As the presence of garnet in the residue is not consistent with the unfractionated melt inclusion patterns, the required depletion for the less incompatible-elements may reflect either: (1) low values of the bulk partition coefficients used in the pHMELTS calculations (McKenzie and O'Nions, 1991, 1995; Wood and Blundy, 1997), (2) a natural depletion of these elements beneath the FAMOUS zone, or (3) a very low proportion of melts produced from garnet-bearing peridotite. Note, however, that major-element compositions of the peridotite source considered in the calculations preclude much melting in the garnet stability field at realistic mantle temperatures (~1250–1400 °C). Hence our results suggest that, contrary to major-elements, most of the variation in the trace-element compositions (Fig. 13) and trace-element ratios (Fig. 14) in the melt inclusions can be accounted for by isentropic continuous melting.

5.3.3. Crossing of the trace-element patterns

Although progressive melting can be considered as a plausible explanation for most of the trace-element characteristics of the melt inclusions, it does not provide a clear solution to a major problem of the melt inclusion data: crossing of the trace-element patterns. During progressive melting in the garnet stability field, crossing of REE patterns occurs between M- and HREE (around Eu–Dy, depending on the values used for the partition coefficients), because HREE have high garnet-melt partition coefficients. However, in the inclusion patterns, the crossing is irregular and not only restricted to HREE (Fig. 5). Instead, it could reflect several combined effects of entrapment of melts derived from different depths, mixing of different melt batches and different degrees of pre-entrapment olivine crystallization. Such a combination of processes is close to the "dynamic melting model" defined by Langmuir et al. (1977) to explain the compositional variability in the FAMOUS whole rocks and the associated crossing REE patterns. In this process, melts are derived from different parts and at different degrees of melting of the source region. Crossing of REE patterns can thus be a consequence of mixing of melt batches with different degrees of incompatible trace-element enrichment.

5.3.4. Major- and trace-element decoupling

Among crucial features of the melt inclusion data, the lack of correlation between major and trace elements (although good correlations are observed within each

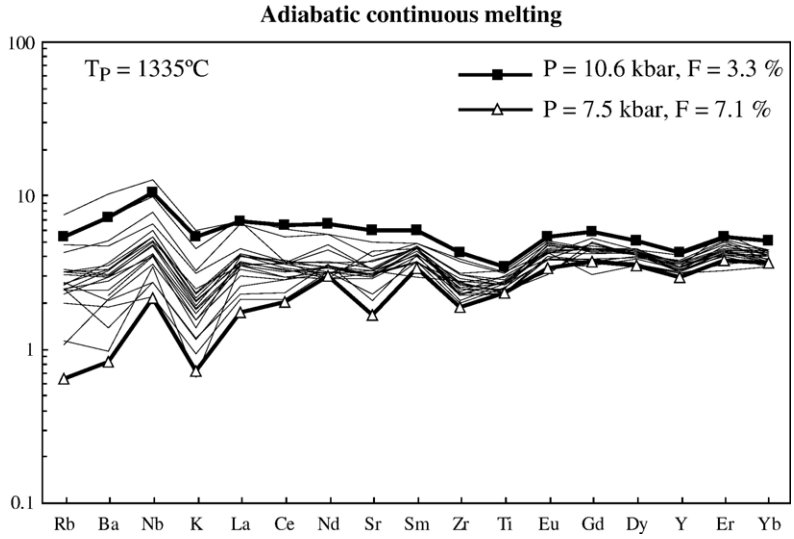

Fig. 13. Primitive mantle-normalized diagram (Sun and McDonough, 1989) showing trace-element data for olivine-hosted melt inclusions in sample ARP73–10–03 and for pHMELTS model melts. Two compositions of instantaneous melts produced by isentropic continuous melting which have been extracted at different pressures and degrees of melting are shown to frame the compositional field of the melt inclusions. For this calculation, potential temperature is 1335 °C. The composition of the source is reported in Table 1. Oxygen fugacity is equal to QFM and 2% of melt is retained in the residue.

group of elements) raises probably the most important problem. This apparent decoupling, which has also been observed for the FAMOUS whole rocks (Langmuir et al., 1977; Bryan, 1979), may be due to the fact that major and trace elements in melts are not governed by the same physical or chemical parameters. Accordingly, the superimposition of the different processes involved in MORB petrogenesis (source heterogeneity, polybaric continuous melting, mixing of melt increments, melt transport, olivine crystallization, etc.) could be recorded differently by the two groups of elements.

As major-elements are the main components of mantle minerals, their behavior is essentially controlled by phase equilibria during melting and thus by the physical P–T conditions in the mantle source region. For instance, contrary to trace elements, it is known that major-elements such as SiO_2 and FeO are strongly dependent on the pressure at the time of melting. On the other hand, incompatible trace elements record information about the source composition which may have been modified by previous melting episodes. In addition, early olivine fractionation and mixing effects are superimposed on those of the melting process and seem to play a significant role in the apparent decoupling of major and trace elements in the melt inclusions. Indeed, an early episode of olivine crystallization before melt entrapment would significantly change major-element abundances in the melt, whereas trace-element contents would all be slightly enriched by the same factor.

5.3.5. Summary on the role of partial melting

To summarize previous sections, progressive isobaric continuous melting of a relatively fertile lherzolite (to account, for example, for the relatively high TiO_2 abundances in the melt inclusions), with mixing to some extent between different melt batches, is a plausible explanation for the observed compositional variations in both major- and trace-element compositions of the olivine-hosted, primitive melt inclusions trapped in the ARP73–10–03 sample. This hypothesis requires that the mantle source is enriched in very incompatible trace elements compared to the DMM source composition of Workman and Hart (2005). On the other hand, the more realistic model of polybaric continuous melting can also account for the melt inclusion data, providing that the source is characterized by a large range in its potential temperature (1280–1395 °C for the DMM source composition of Workman and Hart, 2005) and/or its water content at a small-scale. However, two features of the melt inclusion compositions, namely the crossing of trace-element patterns and the decoupling between major- and trace-element compositions, require a more complex model combining several processes such as continuous partial melting, magma mixing, olivine crystallization, etc. Therefore, melt inclusions are thought to sample liquids that are derived from different depths and different degrees of continuous partial melting from a source which is rather homogeneous in composition (except perhaps in its H_2O content) but probably heterogeneous in temperature. These

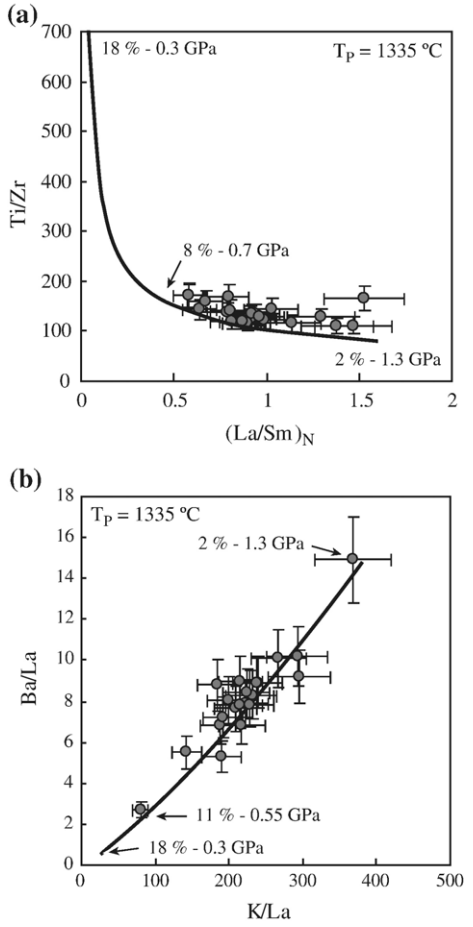

Fig. 14. Ti/Zr vs $(La/Sm)_N$ and Ba/La vs K/La in melt inclusions (shaded circles) and in pHMELTS model liquids (curve). La/Sm ratio (a) is normalized to the composition of chondrite C1 (Sun and McDonough, 1989). Liquids are produced in a model of isentropic continuous melting of the source defined in Table 1. Parameters of the isentropic melting model are the same as in Fig. 13.

increments of melt may then suffer various extents of magma mixing and olivine crystallization before entrapment in the olivine phenocrysts. It is therefore suggested that major and trace elements may record distinctive fingerprints of the processes (segregation, mixing of different melt increments, melt transport, olivine fractionation, etc.) that generated the melt inclusions.

5.4. Variation of the highly incompatible-element ratios: evidence for source heterogeneity?

Ratios of highly incompatible-elements (e.g., Ba/Nb, La/Ce, K/Ba and K/Rb) are more variable in the melt inclusions than in whole rocks. In addition, correlations between ratios of highly incompatible-elements with the same denominator (Fig. 14b) are observed: such correlations could indicate at first sight that the trace-element variations among the melt inclusions reflect a mixing relationship between two mantle sources. However, the different melting models show that in the case of continuous melting (and even more in the case of 'pure' fractional melting), caution is required when attempting to interpret incompatible trace-element ratios in terms of present-day mantle source ratios. Indeed a small difference in the bulk partition coefficients of two elements could produce a large variation of their ratio during partial melting, depending on the range of the degree of melting. This is illustrated in Fig. 14b, where the observed Ba/La versus K/La correlation for the melt inclusions is consistent with an isentropic continuous melting process in the range of ~2–11% and ~1.3–0.55 GPa. Therefore, although a small and local chemical heterogeneity of the source cannot be fully rejected on the basis of our results, it is suggested that partial melting is the main cause of the observed compositional variations.

5.5. Physical implications

It has been proposed that liquid can be extracted at very low melt fractions during melting and that melt interconnectivity is established for melt fractions of < 1 vol.% (Kohlstedt, 1992). A consequence is that melt migration through the mantle could occur by porous flow (McKenzie, 1984; Spiegelman and McKenzie, 1987). In this case, and as discussed in Section 5.2, liquid should approach equilibrium with minerals in the matrix (Navon and Stolper, 1987). However it is known that melts are often transported to the crust without re-equilibration with the surrounding mantle, since major- and trace-element compositions in MORB are not in equilibrium with lherzolitic and harzburgitic residues at low pressures (Stolper, 1980; Christie et al., 1986; Johnson et al., 1990). Therefore rapid segregation and migration of magmas are required beneath mid-ocean ridges, with melt transport by focused flow in channels (Sleep, 1988; Stevenson, 1989; Kelemen et al., 1995a,b, 1997; Spiegelman and Kelemen, 2003) or fractal tree distribution (Hart, 1993). Indeed dunite residues found in ophiolites can be reproduced by models of reactive melt transport through the mantle with focused flow in channels (Kelemen et al., 1995a; Asimow and Stolper, 1999; Spiegelman et al., 2001; Spiegelman and Kelemen, 2003; Morgan and Liang, 2005). Such reactions occur by preferential dissolution of pyroxene which produces melt and olivine (Kelemen, 1990; Kelemen et al., 1990, 1995b; Spiegelman et al., 2001). As the permeability and porosity are increased by this reaction, the melt flux is enhanced and high-permeability dissolution channels are formed.

The coexistence, at the site of the host phase crystallization, of chemically distinct melts preserved in phenocrysts from the ARP73–10–03 MORB sample provides important constraints on the physics of melt segregation and transport beneath the FAMOUS ridge. It requires efficient segregation of melts from their source region. No evidence of diffusive re-equilibration with the surrounding mantle is found in the melt inclusion data, which suggests an ascent to the site of olivine crystallization without extensive interaction. The observation of a large chemical variability at small-scale in melt inclusions from a single sample (Sobolev and Shimizu, 1993a; Shimizu, 1998; Slater et al., 2001) or in MORB lavas (Reynolds et al., 1992; Perfit et al., 1994; Reynolds and Langmuir, 2000) strongly suggests that melt transport does not readily homogenize melt compositions under mid-ocean ridges. Spiegelman and Kelemen (2003) argued that a physical system that extracts melts from different depths without allowing them to mix during transport through the mantle is required to interpret melt inclusions as instantaneous dynamic melts trapped in olivine near the MOHO. They thus proposed that melt transport through a channel network transpose the vertical variability produced by polybaric melting for highly incompatible-elements into horizontal variability across individual channels. This mechanism, which may therefore produce highly variable melt compositions on small length scales and limit interaction between solid and liquid, cannot be rejected from our data. Finally, our observations indicate that melt inclusions trapped within early-formed minerals offer a means of accessing high pressure information which has been partially obliterated in MORB lavas.

6. Conclusions

Silicate melt inclusions in primitive minerals provide access to the early history of mantle magmas since entrapment isolates them from the complex differentiation and mixing processes that occur at shallower levels (Sobolev, 1996; Schiano, 2003). Specifically, primitive melt inclusions in MORB phenocrysts provide further constraints on melting processes, melt transport and mantle source compositions beneath mid-ocean ridges.

The large variations in the major- and trace-element concentrations in melt inclusions trapped in olivine phenocrysts ($Fo_{87.2–91.3}$) from a MORB from the FAMOUS area can be accounted for by partial melting of a relatively homogeneous mantle source and subsequent mixing in various proportions of the melt batches produced at different degrees of melting and/or in different parts of the melting system. The evolution of the melt inclusion compositions cannot be reconciled with trends calculated for mantle-melt chemical exchange during reactive transport, suggesting that the trapped melts are able to preserve pristine information about the melting conditions. These observations imply that distinct magma batches must be transported from their melting depths to the site of olivine crystallization without significant exchange with the surrounding mantle.

Acknowledgements

We would like to thank C.H. Langmuir for providing us with his program of polybaric melting. Technical assistance provided by M. Veschambre and J.-L. Devidal with the electron microprobe was greatly appreciated. Constructive reviews were provided by A.A. Gurenko and an anonymous reviewer. This research was conducted with partial support from the European Community's Human Potential Program under contract HPRN-CT-2002–00211 (Euromelt).

Appendix A

Correction for post-entrapment overgrowth of the host olivine at the inclusion walls during cooling was carried out numerically by dissolving 0.1 wt.% increments of olivine into the liquid. The evaluation of the equilibrium value of $K_{DOl-liq}^{Fe-Mg}$ was done by applying a model that incorporates the effects of melt composition (in particular SiO_2 and alkalis) and temperature on Fe–Mg partitioning (Toplis, 2005). Homogenization temperature of the melt inclusions (1270–1300 °C) was taken as an estimate of the temperature of equilibrium in the system. The starting composition of olivine was that in equilibrium with the melt inclusion; after each dissolution increment, the olivine composition in equilibrium with the corrected melt composition was computed and was used in the next dissolution step. The procedure was stopped once the corrected melt composition was in equilibrium with the host olivine: on average, dissolution of ~13 wt.% olivine was necessary to reach this equilibrium. The amount of post-entrapment crystallization ($X_C = \frac{X_d}{X_d+1}$; where X_d is the amount of olivine dissolution in the melt) is given for each analysis in Table S1 in supplementary data. The value $Fe^{3+}/\Sigma Fe$ was chosen equal to 0.07 (Christie et al., 1986) in the analyzed melt and Fe^{3+} was assumed to behave as an incompatible-element during olivine crystallization, so that the oxidation state evolved during the calculations. Knowing the amount of post-entrapment olivine crystallization, it was then possible to calculate the trace-element compositions at the time of entrapment.

Appendix B

Pearson Product–Moment Correlation between major- and trace-element data in the melt inclusions. This correlation reflects the degree of linear relationship between two variables. It ranges from +1 to −1. A correlation of +1 means that there is a perfect positive linear relationship between variables

	SiO_2	TiO_2	Al_2O_3	MnO	FeO*	MgO	CaO	Na_2O	K_2O	Cl	S	Li	Be	B	F	K	Sc	Ti	V
SiO_2	1																		
TiO_2	0.53	1																	
Al_2O_3	0.26	0.09	1																
MnO	−0.38	−0.33	−0.08	1															
FeO*	−0.85	−0.64	−0.22	0.32	1														
MgO	−0.13	−0.01	−0.52	−0.25	−0.16	1													
CaO	−0.04	0.05	−0.09	0.18	−0.06	−0.42	1												
Na_2O	0.52	0.63	0.04	−0.13	−0.59	0.14	−0.39	1											
K_2O	0.39	0.30	0.37	0.13	−0.39	−0.34	0.08	0.24	1										
Cl	0.22	0.23	0.25	0.02	−0.22	−0.12	−0.21	0.31	0.79	1									
S	0.30	0.11	−0.48	0.10	−0.20	0.13	−0.08	0.39	0.00	0.01	1								
Li	0.09	0.04	−0.11	0.06	−0.06	0.12	−0.21	0.25	−0.38	−0.42	0.22	1							
Be	0.56	0.42	−0.03	−0.25	−0.61	0.29	−0.15	0.34	0.35	0.28	0.10	−0.12	1						
B	0.53	0.44	0.36	−0.03	−0.54	−0.31	0.21	0.33	0.49	0.22	−0.14	−0.16	0.15	1					
F	0.14	0.20	0.01	0.00	−0.17	0.06	−0.06	0.11	0.22	0.16	−0.37	−0.20	0.48	0.35	1				
K	0.40	0.28	0.34	0.08	−0.35	−0.36	0.10	0.21	0.96	0.73	−0.03	−0.42	0.33	0.49	0.21	1			
Sc	−0.44	−0.19	−0.34	0.31	0.49	−0.36	0.64	−0.48	−0.12	−0.32	0.11	0.03	−0.38	−0.33	−0.30	−0.10	1		
Ti	0.46	0.84	−0.07	−0.27	−0.60	0.01	0.25	0.51	0.31	0.20	0.17	−0.08	0.53	0.32	0.14	0.28	0.07	1	
V	−0.25	−0.31	0.07	0.04	0.37	−0.20	0.07	−0.31	−0.29	−0.31	−0.31	0.30	−0.20	−0.18	0.09	−0.32	0.39	−0.08	1
Cr	−0.05	−0.20	−0.14	0.05	−0.04	0.39	−0.21	−0.08	−0.10	0.18	−0.10	−0.25	0.32	−0.18	0.51	−0.17	−0.42	−0.20	−0.09
Rb	0.37	0.19	0.28	0.02	−0.31	−0.34	0.20	0.11	0.86	0.56	0.00	−0.45	0.38	0.25	0.16	0.90	0.04	0.32	−0.26
Sr	0.26	0.51	0.27	0.12	−0.31	−0.32	0.22	0.20	0.71	0.47	−0.20	−0.43	0.26	0.56	0.36	0.76	−0.01	0.46	−0.19
Y	0.37	0.57	0.15	−0.35	−0.35	0.05	−0.29	0.48	0.14	0.21	−0.03	−0.04	0.63	0.17	0.49	0.09	−0.29	0.59	0.25
Zr	0.09	0.56	−0.06	−0.11	−0.19	−0.18	0.43	0.15	0.22	0.12	−0.03	−0.21	0.01	0.24	−0.07	0.30	0.28	0.60	−0.19
Nb	0.31	0.29	0.31	0.09	−0.29	−0.35	0.15	0.13	0.94	0.73	−0.08	−0.47	0.28	0.47	0.21	0.98	−0.06	0.28	−0.29
Cs	0.20	0.30	0.37	0.13	−0.44	0.02	0.13	0.13	0.37	0.28	−0.34	−0.41	0.36	0.40	0.26	0.36	−0.36	0.37	−0.30
Ba	0.36	0.26	0.28	0.08	−0.33	−0.33	0.13	0.16	0.95	0.72	0.00	−0.44	0.36	0.46	0.21	0.99	−0.07	0.29	−0.31
La	0.27	0.43	0.24	0.06	−0.28	−0.38	0.33	0.12	0.83	0.61	−0.11	−0.48	0.23	0.48	0.16	0.88	0.08	0.45	−0.29
Ce	0.17	0.50	0.13	−0.01	−0.27	−0.27	0.40	0.13	0.56	0.42	−0.05	−0.47	0.07	0.40	−0.01	0.62	0.13	0.50	−0.36
Nd	0.10	0.51	−0.16	−0.22	−0.26	0.00	0.47	0.09	0.12	0.08	0.04	−0.33	0.23	0.14	−0.16	0.20	0.25	0.68	−0.30
Sm	0.40	0.52	0.45	−0.21	−0.37	−0.32	0.05	0.27	0.36	0.33	−0.16	−0.28	0.49	0.42	0.12	0.32	−0.20	0.61	−0.03
Eu	0.13	0.29	−0.32	−0.03	−0.27	0.27	0.22	0.12	−0.05	−0.17	0.13	−0.08	0.44	0.22	0.08	−0.03	0.12	0.58	0.20
Gd	0.48	0.38	0.56	−0.27	−0.39	−0.25	−0.22	0.28	0.49	0.45	−0.13	−0.10	0.54	0.28	0.04	0.45	−0.31	0.44	−0.06
Dy	0.46	0.37	0.25	−0.33	−0.36	−0.12	−0.11	0.27	0.20	0.25	−0.07	−0.07	0.56	0.36	0.18	0.11	−0.28	0.51	0.18
Er	0.02	0.33	0.32	−0.23	−0.11	−0.14	−0.05	0.28	0.20	0.24	−0.37	−0.18	0.38	0.18	0.39	0.20	−0.15	0.47	0.27
Yb	0.38	0.57	0.23	−0.12	−0.38	−0.10	−0.20	0.59	0.07	0.22	0.02	0.24	0.34	0.33	0.11	0.03	−0.27	0.59	0.19

(continued on next page)

Appendix B (*continued*)

	Cr	Rb	Sr	Y	Zr	Nb	Cs	Ba	La	Ce	Nd	Sm	Eu	Gd	Dy	Er
SiO_2																
TiO_2																
Al_2O_3																
MnO																
FeO*																
MgO																
CaO																
Na_2O																
K_2O																
Cl																
S																
Li																
Be																
B																
F																
K																
Sc																
Ti																
V																
Cr	1															
Rb	−0.11	1														
Sr	−0.29	0.61	1													
Y	0.15	0.09	0.30	1												
Zr	−0.52	0.27	0.66	0.13	1											
Nb	−0.16	0.87	0.81	0.10	0.38	1										
Cs	0.27	0.40	0.40	0.10	0.23	0.37	1									
Ba	−0.13	0.92	0.73	0.09	0.27	0.98	0.35	1								
La	−0.29	0.77	0.89	0.13	0.66	0.93	0.40	0.87	1							
Ce	−0.41	0.51	0.84	0.08	0.89	0.70	0.36	0.60	0.89	1						
Nd	−0.40	0.26	0.46	0.12	0.86	0.24	0.34	0.20	0.51	0.74	1					
Sm	−0.18	0.27	0.46	0.59	0.42	0.32	0.49	0.31	0.45	0.45	0.54	1				
Eu	−0.12	0.01	0.22	0.40	0.25	0.00	0.22	0.02	0.10	0.17	0.48	0.38	1			
Gd	−0.17	0.42	0.27	0.46	0.09	0.37	0.40	0.43	0.32	0.16	0.24	0.80	0.13	1		
Dy	0.00	0.05	0.12	0.63	0.03	0.08	0.27	0.12	0.11	0.02	0.23	0.82	0.45	0.77	1	
Er	0.07	0.38	0.27	0.64	0.23	0.21	0.42	0.21	0.27	0.19	0.27	0.63	0.26	0.49	0.52	1
Yb	−0.19	−0.11	0.24	0.65	0.28	0.00	0.24	−0.01	0.09	0.15	0.30	0.72	0.43	0.59	0.72	0.51

Appendix C

Mineral/melt partition coefficients used in the pHMELTS calculations

	Olivine	cpx	opx	Garnet	spl	Feldspar
Na	0.00001	var.	0.05	0.04		var.
K	0.00018	var.	0.001	0.001	0.0001	var.
Cr	0.3	3	1.5	5.5	300	0.05
Mn	0.5	0.44	0.7	2.05	0.25	0.05
Rb	0.00018	var.	0.0006	0.0007	0.0001	var.
Ba	0.0003	var.	0.0001	1.00E-05	0.0001	var.
Nb	0.005	0.02	0.005	0.07		0.01
La	0.0004	var.	0.002	var.	0.01	var.
Ce	0.0005	var.	0.003	var.	0.01	var.
Nd	0.001	var.	0.0068	var.	0.01	var.
Sr	0.00019	var.	0.007	6.00E-04		var.
Sm	0.0013	var.	0.01	var.	0.01	var.
Zr	0.01	0.1	0.03	0.32		0.01
Ti	0.02	0.18	0.1	0.28	0.15	0.04
Eu	0.0016	var.	0.013	var.	0.01	var.
Gd	0.0015	var.	0.016	var.	0.01	var.
Dy	0.0017	var.	0.022	var.	0.01	var.
Y	0.005	var.	0.005	var.		var.
Er	0.0015	var.	0.03	var.	0.01	var.
Yb	0.0015	var.	0.049	var.	0.01	var.
H_2O	0.0004	0.004	0.002	0.0004		0.0005

Constant default mineral/melt partition coefficients are taken from the compilations of McKenzie and O'Nions (1991, 1995). Variable mineral/melt partition coefficients (var; $D=D(P, T, X)$) are defined from the method of Wood and Blundy (1997) and are taken from Wood and Blundy (1997), Blundy et al. (1995) and Wood et al. (1999) for clinopyroxene (cpx), van Westrenen et al. (1999) for garnet, and Blundy and Wood (1994) for feldspar.

Appendix D. Supplementary data

Supplementary data associated with this article can be found, in the online version, at 10.1016/j.chemgeo.2007.02.002.

References

Allègre, C.J., Turcotte, D.L., 1986. Implications for a two component marble-cake mantle. Nature 323, 123–127.

Asimow, P.D., Dixon, J.E., Langmuir, C.H., 2004. A hydrous melting and fractionation model for mid-ocean ridge basalts: application to the Mid-Atlantic Ridge near the Azores. Geochem. Geophys. Geosyst. 5 (Q01E16). doi:10.1029/2003GC000568.

Asimow, P.D., Stolper, E.M., 1999. Steady-state mantle-melt interactions in one dimension: I. Equilibrium transport and melt focusing. J. Petrol. 40, 475–494.

Baker, M.B., Hirschmann, M.M., Ghiorso, M.S., Stolper, E.M., 1995. Compositions of near-solidus peridotite melts from experiments and thermodynamic calculations. Nature 375, 308–311.

Baronnet, A., 1984. Growth kinetics of the silicates. A review of basic concepts. Fortschr. Mineral. 62, 187–232.

Bender, J.F., Hodges, F.N., Bence, A.E., 1978. Petrogenesis of basalts from the project Famous area: experimental study from 0 to 15 kbars. Earth Planet. Sci. Lett. 41, 277–302.

Blundy, J.D., Falloon, T.J., Wood, B.J., Dalton, J.A., 1995. Sodium partitioning between clinopyroxene and silicate melts. J. Geophys. Res. 100, 15501–15515.

Blundy, J.D., Wood, B.J., 1994. Prediction of crystal-melt partition coefficients from elastic moduli. Nature 372, 452–454.

Bottazzi, P., Ottolini, L., Vannucci, R., Zanetti, A., 1994. An accurate procedure for the quantification of rare-earth elements in silicates. In: Chichester, J.W.S. (Ed.), Secondary Ion Mass Spectrometry SIMS IX.

Bryan, W.B., 1979. Regional variation and petrogenesis of basalt glasses from the FAMOUS area, Mid-Atlantic Ridge. J. Petrol. 20, 293–325.

Christie, D.M., Carmichael, I.S.E., Langmuir, C.H., 1986. Oxidation states of mid-ocean ridge basalt glasses. Earth Planet. Sci. Lett. 79, 379–411.

Danyushevsky, L.V., Della-Pasqua, F.N., Sokolov, S., 2000. Re-equilibration of melt inclusions trapped by magnesian olivine phenocrysts from subduction-related magmas: petrological implications. Contrib. Mineral. Petrol. 138, 68–83.

Danyushevsky, L.V., Leslie, R.A.J., Crawford, A.J., Durance, P., 2004. Melt inclusions in primitive olivine phenocrysts: the role of localized reaction processes in the origin of anomalous compositions. J. Petrol. 45, 2531–2553.

de Hoog, J.C.M., Koestsier, G.W., Bronto, S., Sriwana, T., van Bergen, M.J., 2001. Sulfur and chlorine degassing from primitive arc magmas: temporal changes during the 1982–1983 eruptions of Galunggung (West Java, Indonesia). J. Volcanol. Geotherm. Res. 108, 55–83.

DePaolo, D.J., 1981. Trace-element and isotopic effects of combined wall-rock assimilation and fractional crystallization. Earth Planet. Sci. Lett. 1981 (53), 189–202.

Dixon, J.E., Clague, D.A., Stolper, E., 1991. Degassing history of water, sulphur and carbon in submarine lavas vrom Kilauea volcano, Hawaii. J. Geol. 99, 371–394.

Dosso, L., Bougault, H., Langmuir, C.H., Bollinger, C., Bonnier, O., Etoubleau, J., 1999. The age and distribution of mantle heterogeneity along the Mid-Atlantic Ridge (31–41°N). Earth Planet. Sci. Lett. 170, 269–286.

Dupré, B., Lambret, B., Rousseau, D., Allègre, C.J., 1981. Limitations on the scale of mantle heterogeneities under oceanic ridges. Nature 294, 552–554.

Falloon, T.J., Danyushevsky, L.V., Green, D.H., 2001. Peridotite melting at 1 GPa: reversal experiments on partial melt compositions produced by peridotite-basalt sandwich experiments. J. Petrol. 42, 2363–2390.

Frey, F.A., Walker, N., Stakes, D., Hart, S.R., Nielsen, R., 1993. Geochemical characteristics of basaltic glasses from the AMAR and FAMOUS axial valleys, Mid-Atlantic Ridge (36–37°N): petrogenetic implications. Earth Planet. Sci. Lett. 115, 117–136.

Gaetani, G.A., Watson, E.B., 2002. Modeling the major-element evolution of olivine-hosted melt inclusions. Chem. Geol. 183, 25–41.

Gaetani, G.A., Cherniak, D.J., Watson, E.B., 2002. Diffusive reequilibration of CaO in olivine-hosted melt inclusions. Abstracts of the 12th annual V. M. Goldschmidt conference. Geochim. Cosmochim. Acta 66 (15A), 254.

Gaetani, G.A., Watson, E.B., 2000. Open system behavior of olivine-hosted melt inclusions. Earth Planet. Sci. Lett. 183, 27–41.

Gannoun, A., Burton, K.W., Thomas, L.E., Parkinson, I.J., Calsteren, P.V., Schiano, P., 2004. Osmium isotope heterogeneity in the constituent phases of mid-ocean ridge basalts. Science 303, 70–72.

Ghiorso, M.S., Hirschmann, M.M., Reiners, P.W., Kress, V.C.I., 2002. The pMELTS: a revision of MELTS for improved calculation of phase relations and major-element partitioning related to partial melting of the mantle to 3 GPa. Geochem. Geophys. Geosyst. 3. doi:10.1029/2001GC000217.

Ghiorso, M.S., Sack, R.O., 1995. Chemical mass transfer in magmatic processes. 4. A revised and internally consistent thermodynamic model for the interpolation and extrapolation of liquid-solid equilibria in magmatic systems at elevated temperatures and pressures. Contrib. Mineral. Petrol. 119, 197–212.

Hart, S.R., 1993. Equilibrium during mantle melting: a fractal tree model. Proc. Natl. Acad. Sci. 90, 11914–11918.

Hirschmann, M.M., Baker, M.B., Stolper, E.M., 1998. The effects of alkalis on the silica content of mantle-derived melts. Geochim. Cosmochim. Acta 62, 883–902.

Hofmann, A.W., 1988. Chemical differentiation of the Earth: the relationship between mantle, continental crust, and oceanic crust. Earth Planet. Sci. Lett. 90, 297–314.

Johnson, K.T., Dick, H.J.B., Shimizu, N., 1990. Melting in the oceanic upper mantle: an ion microprobe study of diopsides in abyssal peridotites. J. Geophys. Res. 95, 2661–2678.

Jurewicz, A.J.G., Watson, E.B., 1988. Cations in olivines. 2. Diffusion in olivine xenocryst, with applications to petrology and mineral physics. Contrib. Mineral. Petrol. 99, 186–201.

Kamenetsky, V., Crawford, A.J., 1998. Melt-peridotite reaction recorded in the chemistry of spinel and melt inclusions in basalt from 43°N, Mid-Atlantic Ridge. Earth Planet. Sci. Lett. 164, 345–352.

Kamenetsky, V., 1996. Methodology for the study of melt inclusions in Cr-spinel, and implications for parental melts of MORB from FAMOUS area. Earth Planet. Sci. Lett. 142, 479–486.

Kelemen, P.B., 1990. Reaction between ultramafic rock and fractionating basaltic magma, 1, Phase-relations, the origin of calc-alkaline magma series, and the formation of discordant dunite. J. Petrol. 31, 51–98.

Kelemen, P.B., Joyce, D.B., Webster, J.D., Holloway, J.R., 1990. Reaction between ultramafic rock and fractionating basaltic magma, 2, experimental investigation of reaction between olivine

tholeiite and harzburgite at 1150 °C–1050 °C and 5 kb. J. Petrol. 31, 99–134.
Kelemen, P.B., Shimizu, N., Salters, V.J.M., 1995a. Extraction of mid-ocean-ridge basalt from the upwelling mantle by focused flow of melt in dunite channels. Nature 375, 747–753.
Kelemen, P.B., Whitehead, J.A., Aharonov, E., Jordahl, K.A., 1995b. Experiments on flow focusing in soluble porous media, with applications to melt extraction from the mantle. J. Geophys. Res. 100, 475–496.
Kelemen, P.B., Hirth, G., Shimizu, N., Spiegelman, M., Dick, H.J.B., 1997. A review of melt migration processes in the adiabatically upwelling mantle beneath spreading ridges. Philos. Trans. R. Soc. Lond., A 355, 283–318.
Klein, E.M., Langmuir, C.H., 1987. Global correlations of ocean ridge basalt chemistry with axial depth and crustal thickness. J. Geophys. Res. 92, 8089–8115.
Kohlstedt, D.L., 1992. Structure, rheology and permeability of partially molten rocks at low melt fractions. In: Phipps Morgan, J., Blackman, D.K., Sinton, J.M. (Eds.), Mantle Flow and Melt Generation at Mid-Ocean Ridges. Geophys. Mon. Am. Geophys. Union, pp. 183–280.
Kushiro, I., 1996. Partial melting of a fertile mantle peridotite at high pressures: an experimental study using aggregates of diamond. In: Basu, A., Hart, S. (Eds.), Earth Processes: Reading the Isotopic Code. Geophys. Monograph. American Geophysical Union, pp. 109–122.
Langmuir, C.H., Klein, E.M., Plank, T., 1992. Petrological systematics of mid-ocean ridge basalts: constraints on melt generation beneath ocean ridges. In: Phipps Morgan, J., Blackman, D.K., Sinton, J.M. (Eds.), Mantle Flow and Melt Generation at Mid-Ocean Ridges. Geophys. Mon. Am. Geophys. Union, pp. 183–280.
Langmuir, C.H., Bender, J.F., Bence, A.E., Hanson, G.N., Taylor, S.R., 1977. Petrogenesis of basalts from the FAMOUS area: Mid-Atlantic Ridge. Earth Planet. Sci. Lett. 36, 133–156.
Laporte, D., Toplis, M.M.S., Devidal, J.-L., 2004. A new experimental technique for extracting liquids from peridotite at very low degrees of melting: application to partial melting of depleted peridotite. Contrib. Mineral. Petrol. 146 (4), 463–484.
Le Roex, A.P., Erlank, A.J., Needham, H.D., 1981. Geochemical and mineralogical evidence for the occurrence of at least three distinct magma types in the “Famous” region. Contrib. Mineral. Petrol. 77, 24–37.
McKenzie, D.P., O’Nions, R.K., 1995. The source regions of ocean island basalts. J. Petrol. 36, 133–159.
McKenzie, D.P., O’Nions, R.K., 1991. Partial melt distribution from inversion of rare-earth element concentrations. J. Petrol. 32, 1021–1091.
McKenzie, D.P., Bickle, M.J., 1988. The volume and composition of melt generated by extension of the lithosphere. J. Petrol. 29, 625–679.
McKenzie, D.P., 1984. The generation and compaction of partial melts. J. Petrol. 25, 713–765.
Médard, E., Schmidt, M.W., Schiano, P., 2004. Liquidus surfaces of ultracalcic primitive melts: formation conditions and sources. Contrib. Mineral. Petrol. 148, 201–215.
Messiga, B., Tribuzio, R., Bottazzi, P., Ottolini, L., 1995. An ion microprobe study of trace-element composition of clinopyroxenes from blueschist and eclogitized Fe–Ti–gabbros, Ligurian Alps, northwestern Italy: some petrologic considerations. Geochim. Cosmochim. Acta 59, 59–75.
Metrich, N., Clocchiatti, R., 1989. Melt inclusion investigation of the volatile behaviour in historic alkali basaltic magmas of Etna. Bull. Volcanol. 51, 185–198.
Metrich, N., Clocchiatti, R., 1996. Sulfur abundance and its speciation in oxidised alkaline melts. Geochim. Cosmochim. Acta 60, 4151–4160.
Metrich, N., Rutherford, M.J., 1992. Experimental study of chlorine behavior in hydrous silicic melts. Geochim. Cosmochim. Acta 56, 607–616.
Metrich, N., Sigurdsson, H., Meyer, P.S., Devine, J.D., 1991. The 1783 Lakagigar eruption in Iceland; geochemistry, CO (sub 2) and sulfur degassing. Contrib. Mineral. Petrol. 107, 435–447.
Morgan, Z., Liang, Y., 2005. An experimental study of the kinetics of lherzolite reactive dissolution with applications to melt channel formation. Contrib. Mineral. Petrol. 150, 369–385.
Navon, O., Stolper, E.M., 1987. Geochemical consequences of melt percolation: the upper mantle as a chromatographic column. J. Geol. 95, 285–307.
Niu, Y., Batiza, R., 1991. An empirical method for calculating melt compositions produced beneath mid-ocean ridges: application to axis and off-axis (seamounts) melting. J. Geophys. Res. 96, 21753–21777.
Niu, Y., Batiza, R., 1993. Chemical variation trends at fast and slow spreading mid-ocean ridges. J. Geophys. Res. 98, 7887–7902.
Oskarsson, N., Sigvaldason, G.E., Steinthorsson, S., 1982. A dynamic model of rift zone petrogenesis and the regional petrology of Iceland. J. Petrol. 23, 28–74.
Ottolini, L., Bottazzi, P., Vannucci, R., 1993. Quantification of lithium, beryllium, and boron in silicates by secondary ion mass spectrometry using conventional energy filtering. Anal. Chem. 65, 1960–1968.
Ottolini, L., Bottazzi, P., Zanetti, A., 1994. Quantitative analysis of hydrogen, fluorine and chlorine in silicates using energy filtering. In: Benninghoven, A., Nihei, Y., Shimizu, R., Werner, H.W. (Eds.), Secondary Ion Mass Spectrometry SIMS IX. John Wiley & Sons.
Palais, J.M., Sigurdsson, H., 1989. Petrologic evidence of volatile emissions from major historic and pre-historic volcanic eruptions. In: Berger, A., Dickinson, R.E., Kidson, J.W. (Eds.), Understanding Climate Change. Geophysical Monograph. Am. Geophys. Union, Washington, DC, pp. 31–53.
Perfit, M.R., Fornari, D.J., Smith, M.C., Bender, J.F., Langmuir, C.H., Haymon, R.M., 1994. Small-scale spatial and temporal variations in mid-ocean ridge crest magmatic processes. Geology 22, 375–397.
Pickering-Witter, J., Johnston, A.D., 2000. The effects of variable bulk composition on the melting systematics of fertile peridotitic assemblages. Contrib. Mineral. Petrol. 140, 190–211.
Plank, T., Langmuir, C.H., 1992. Effects of the melting regime on the composition of oceanic crust. J. Geophys. Res. 97, 19749–19770.
Presnall, D.C., Gudfinnsson, G.H., Walter, M.J., 2002. Generation of mid-ocean ridge basalts at pressures from 1 to 7 GPa. Geochim. Cosmochim. Acta 66, 2073–2090.
Reiners, P.W., 1998. Reactive melt transport in the mantle and geochemical signatures of mantle-derived magmas. J. Petrol. 39, 1039–1061.
Reynolds, J.R., Langmuir, C.H., 2000. Identification and implications of off-axis lava flows around the East- Pacific Rise. Geochem. Geophys. Geosyst. 1 (6).
Reynolds, J.R., Langmuir, C.H., Bender, J.F., Kastens, K.A., Ryan, W.B.F., 1992. Spatial and temporal variability in the geochemistry of basalts from the East Pacific Rise. Nature 359, 493–499.
Roeder, P.L., Emslie, R.F., 1970. Olivine–liquid equilibrium. Contrib. Mineral. Petrol. 29, 275–289.
Roy-Barman, M., Wassenburg, G.J., Papanastassiou, D.A., Chaussidon, M., 1998. Osmium isotopic compositions and Re–Os

concentrations in sulfide globules from basaltic glasses. Earth Planet. Sci. Lett. 154, 331–347.
Salters, V.J., Hart, S.R., 1989. The hafnium paradox and the role of garnet in the source of mid-ocean-ridge basalts. Nature 342, 420–422.
Schiano, P., 2003. Primitive mantle magmas recorded as silicate melt inclusions in igneous minerals. Earth-Sci. Rev. 63, 121–144.
Schiano, P., Birck, J.-L., Allègre, C.J., 1997. Osmium–Strontium–Neodymium–Lead isotopic covariations in mid-ocean ridge basalt glasses and the heterogeneity of the upper mantle. Earth Planet. Sci. Lett. 150, 363–381.
Schiano, P., Eiler, J.M., Hutcheon, I.D., Stolper, E.M., 2000. Primitive CaO-rich, silica-undersaturated melts in island arcs: evidence for the involvement of clinopyroxene-rich lithologies in the petrogenesis of arc magmas. Geochem. Geophys. Geosyst. 1 1999GC000032.
Schilling, J.-G., 1973. Iceland mantle plume: geochemical study of Reykjanes ridge. Nature 242, 565–571.
Schwab, B.E., Johnston, A.D., 2001. Melting systematics of modally variable, compositionally intermediate peridotites and the effects of mineral fertility. J. Petrol. 42, 1789–1811.
Shen, Y., Forsyth, D.W., 1995. Geochemical constraints on initial and final depths of melting beneath mid-ocean ridges. J. Geophys. Res. 100, 2211–2237.
Shimizu, N., 1998. The geochemistry of olivine-hosted melt inclusions in a FAMOUS basalt ALV519–4-1. Phys. Earth Planet. Int. 107, 183–201.
Slater, L., McKenzie, D., Grönvold, K., Shimizu, N., 2001. Melt generation and movement beneath Theistareykir, NE Iceland. J. Petrol. 42, 321–354.
Sleep, N.H., 1988. Tapping of melt by veins and dykes. J. Geophys. Res. 93, 10255–10272.
Smith, P.M., Asimow, P.D., 2005. Adiabat_1ph: A new public front-end to the MELTS, pMELTS, and pHMELTS models. Geochem. Geophys. Geosyst. 6, Q02004.
Sobolev, A.V., 1996. Melt inclusions in minerals as a source of principle petrological information. Petrology 4, 209–220.
Sobolev, A.V., Shimizu, N., 1993a. Ultra-depleted primary melt included in an olivine from the mid-Atlantic ridge. Nature 363, 151–154.
Sobolev, A.V., Shimizu, N., 1993b. Superdepleted melts and oceanic mantle permeability. Trans. Russ. Acad. Sci., Earth-Sci. Sect. 328 (1), 182–188.
Spiegelman, M., Elliot, T., 1993. Consequences of melt transport for uranium series disequilibrium in young lavas. Earth Planet. Sci. Lett. 118, 1–20.
Spiegelman, M., Kelemen, P.B., 2003. Extreme chemical variability as a consequence of channelized melt transport. Geochem. Geophys. Geosyst. 4 2002GC000336.
Spiegelman, M., McKenzie, D.P., 1987. Simple 2-D models for melt extraction at mid-ocean ridges and island arcs. Earth Planet. Sci. Lett. 83, 137–152.
Spiegelman, M., Kelemen, P.B., Aharonov, E., 2001. Causes and consequences of flow organization during melt transport: the reaction infiltration instability in compactible media. J. Geophys. Res. 106, 2061–2077.
Stevenson, D.J., 1989. Spontaneous small-scale melt segregation in partial melts undergoing deformation. Geophys. Res. Lett. 16, 1067–1070.
Stolper, E.M., 1980. A phase diagram for Mid-Ocean Ridge basalts: preliminary results and implications for petrogenesis. Contrib. Mineral. Petrol. 74, 13–27.
Sun, S.-s., McDonough, W.F., 1989. Chemical and isotopic systematics of oceanic basalts: implications for mantle composition and processes. In: Saunders, A.D., N.M.J (Eds.), Magmatism in the Ocean Basins. Geological Society Special Publication, pp. 313–345.
Thordarson, T., Self, S., Oskarsson, N., Huselboch, T., 1996. Sulfur, chorine and fluorine degassing and atmospheric loading by the 1783–1784 AD Laki (Skaftar Fires) eruption in Iceland. Bull. Volcanol. 58, 205–225.
Thornber, C.R., Sherrod, D.R., Siems, D.F., Heliker, C.C., Meeker, G.P., Oscarson, R.L., Kauahikaua, J.P., 2002. Whole rock and glass major-element geochemistry of Kilauea volcano, Hawaii, near vent eruptive products: September 1994 through September 2001. U.S.G.S. Open-File Report, 02–17.
Toplis, M.J., 2005. The thermodynamics of iron and magnesium partitioning between olivine and liquid: criteria for assessing and predicting equilibrium in natural and experimental systems. Contrib. Mineral. Petrol. 149, 22–39.
van Westrenen, W., Blundy, J.D., Wood, B.J., 1999. Crystal-chemical controls on trace-element partitioning between garnet and anhydrous silicate melt. Am. Min. 84, 838–847.
Walker, D., Shibata, T., DeLong, S.E., 1979. Abyssal tholeiites from the oceanographer fracture zone, II: phase equilibria and mixing. Contrib. Mineral. Petrol. 70, 111–125.
Wasylenki, L.E., Baker, M.B., Kent, A.J.R., Stolper, E.M., 2003. Near-solidus melting of the shallow upper mantle: partial melting experiments on depleted peridotite. J. Petrol. 44, 1163–1191.
White, W.M., Bryan, W.B., 1977. Sr-isotope, K, Rb, Cs, Sr, Ba, and rare-earth geochemistry of basalts from the FAMOUS area. Geol. Soc. Am. Bull. 88, 571–576.
Wood, B.J., Blundy, J.D., Robinson, J.A.C., 1999. The role of clinopyroxene in generating U-series disequilibrium during mantle melting. Geochim. Cosmochim. Acta 63, 1613–1620.
Wood, B.J., Blundy, J.D., 1997. A predictive model for rare-earth element partitioning between clinopyroxene and anhydrous silicate melt. Contrib. Mineral. Petrol. 129, 166–181.
Workman, R.K., Hart, S.R., 2005. Major and trace-element composition of the depleted MORB mantle (DMM). Earth Planet. Sci. Lett. 231, 53–72.